SEMMELWEIS EGYETEM

DOKTORI ISKOLA

Ph.D. értekezések

3452.

DEREK NORMAN

Kórélettan és transzlációs medicina
című program

Programvezető: Dr. Benyó Zoltán, egyetemi tanár

Témavezető: Dr. Tigyi Gábor, kutatóprofesszor

Development and mechanistic evaluation of an extended-release LPAR2 agonist as a radiation medical countermeasure

PhD thesis

Derek D. Norman

Semmelweis University Doctoral School

Theoretical and Translational Medicine Division

Supervisor:	Gábor Tigyi, MD, D.Sc
Official reviewers:	Géza Sáfrány, MD, D.Sc Károly Liliom, Ph.D
Head of the Complex Examination Committee:	György Reusz, MD, D.Sc
Members of the Complex Examination Committee:	László Cervenák, Ph.D Mihály Kovács, MD, D.Sc

Budapest
2026

Table of Contents

Abbreviations

Akt	Protein kinase B
ANOVA	Analysis of variance
AQ	Aqueous
ARS	Acute radiation syndrome
ATM	Ataxia telangiectasia mutated
AUC	Area under curve
BSA	Bovine serum albumin
CL_T	Total body clearance time
CL_T/F	Plasma clearance
C_{max}	Maximum plasma concentration
C_t	Plasma concentration time
DBIBB	2-[4-(1,3-Dioxo-1*H*,3*H*-benzoisoquinolin-2-yl)butylsulfamoyl]benzoic acid
DDR	DNA damage response
DMEM	Dulbecco's modified Eagle medium
ELISA	Enzyme-linked immunosorbent assay
ERK	Extracellular signal-regulated kinase
F	Bioavailability
FBS	Fetal bovine serum
GI-ARS	Gastrointestinal acute radiation syndrome
Gy	Gray
H-ARS	Hematopoietic acute radiation syndrome
H&E	Hematoxylin and eosin
HSPC	Hematopoietic stem and progenitor cells
IEX-1	Immediate early response gene 3 (IER3)/immediate early response gene X-1
IF1	F1Fo-ATP synthase inhibitor protein
IS	Internal standard
ISC	Intestinal stem cells
IV	Intravenous

JNK	c-Jun N-terminal kinase
K_{el}	Elimination rate constant
KO	Knockout
Lgr5	Leucine-rich repeat-containing G protein-coupled receptor 5
LPA	Lysophosphatidic acid
LPAR	LPA G Protein-coupled receptor
MAPK	Mitogen-activated protein kinase
ME	Microemulsion
MEF	Mouse embryonic fibroblasts
MRT	Mean plasma residence time
NBF	Neutral buffered formalin
NCA	Non-compartmental analysis
NF-κB	Nuclear factor kappa B
NHP	Non-human primates
OTP	Octadecenyl thiophosphate
PACE	Phospho-antibody cell-based ELISA
PK	Pharmacokinetics
PBS	Phosphate buffered saline
PBI-BM5	Partial body irradiation with 5% bone marrow shielding
PI3K	Phosphoinositide 3-kinase
PP2A	Protein phosphatase 2A
RP-1	Radioprotectin-1
ROS	Reactive oxygen species
RT-qPCR	Reverse transcription quantitative polymerase chain reaction
SC	Subcutaneous
SEM	Standard error of the mean
$t_{1/2}$	Elimination half-life
TBI	Total body irradiation
TFA	Trifluoroacetic acid
T_{max}	Time to reach C_{max}
W/O/W	Water-in-oil-in-water
WT	Wild-type

1. Introduction

1.1 Acute Radiation Syndrome

Acute radiation syndrome (ARS) is a complex, multisystem disorder that develops following exposure to high levels of ionizing radiation over a short period of time. The severity and clinical trajectory of ARS depend on total absorbed dose, dose rate, radiation quality, and the extent of whole-body versus partial-body exposure. Historically, understanding of ARS has been informed by observations from atomic bomb survivors, radiological accidents, and controlled preclinical models (1-3).

Ionizing radiation induces biological injury primarily through the generation of DNA double-strand breaks, either directly through energy deposition in DNA or indirectly via radiolysis of water and subsequent production of reactive oxygen species (ROS) (4). DNA double-strand breaks represent one of the most lethal forms of DNA damage and activate a highly coordinated DNA damage response (DDR). Central to this response is activation of ataxia telangiectasia mutated (ATM) kinase, which phosphorylates downstream effectors including p53, H2AX, and checkpoint kinases to orchestrate cell cycle arrest, DNA repair, senescence, or apoptosis (4, 5).

While DNA damage is the initiating event, the clinical manifestations of ARS arise from dysfunction in highly proliferative tissues that depend on continuous cellular renewal. ARS is traditionally divided into three subsyndromes: hematopoietic (H-ARS), gastrointestinal (GI-ARS), and neurovascular. H-ARS predominates at doses above approximately 2 Gy and is characterized by bone marrow suppression and cytopenias (2, 3, 6, 7). GI-ARS becomes clinically significant at higher exposures, typically above 8–10 Gy, where intestinal epithelial loss contributes substantially to morbidity and mortality (8-10). At extreme doses (>20 Gy), neurovascular compromise leads to rapid cardiovascular collapse and death (11).

Despite significant advances in radiation oncology and emergency preparedness, therapeutic options for ARS remain limited. Hematopoietic growth factors such as filgrastim and pegfilgrastim are FDA-approved for treatment of H-ARS (12, 13). However, these countermeasures approved for H-ARS do not mitigate GI-ARS. The absence of effective gastrointestinal mitigation strategies represents a critical vulnerability in radiation emergency response.

Regarding treatment of radiation exposure, a clear distinction must be made between radioprotectors and radiation mitigators. Radioprotectants function prophylactically, using mechanisms like DNA stabilization and free radical scavenging to prevent initial damage. In contrast, radiation mitigators serve as post-exposure treatments—applied 24 hours or more after the event—to alleviate the severity of injury and support regenerative healing. In the context of accidental nuclear incidents or deliberate radiological events, the absence of effective, field-deployable therapies capable of reducing delayed gastrointestinal injury represents a critical translational gap. Development of pharmacologic agents that can be administered after radiation exposure and meaningfully attenuate tissue injury therefore remains a high priority in radiation medicine. These limitations underscore the need for understanding the mechanism of cell injury and the development of translational mitigation strategies that target tissue resilience rather than solely DNA repair.

1.2 Gastrointestinal injury in acute radiation syndrome

The gastrointestinal tract is among the most radiation-sensitive organ systems due to the rapid turnover of its epithelial lining. Under homeostatic conditions, the intestinal epithelium renews itself every 3–5 days (14). This renewal is sustained by multipotent intestinal stem cells (ISC) residing at the base of crypts of Lieberkühn (15, 16).

Lgr5-positive crypt base columnar cells constitute an actively cycling stem cell population responsible for daily epithelial replenishment (16). These cells are highly sensitive to ionizing radiation. Apoptosis of Lgr5-positive cells peaks within 2–6 hours after exposure, and crypt loss becomes morphologically apparent within 24–72 hours. The nadir of crypt depletion typically occurs between days 3 and 5 post-irradiation (17-19).

Loss of crypt stem cells disrupts the structure of the crypt–villus axis, compromises absorptive capacity, and destabilizes tight junction and adherens junction complexes that maintain intestinal epithelial barrier integrity (20, 21). Barrier breakdown permits translocation of luminal bacteria and endotoxins into systemic circulation, triggering inflammatory cascades, bacteremia, sepsis, and multi-organ failure (8). In murine models, survival correlates closely with the preservation of

functional crypt microcolonies, underscoring the importance of ISC survival as a determinant of GI-ARS outcome (22, 23).

Regeneration following injury depends on surviving stem and progenitor populations. Quiescent reserve ISC, including Bmi1-positive cells located at the +4 position of the crypt, exhibit relative radioresistance and can contribute to regeneration (24, 25). More recently, revival stem cells, characterized by clusterin expression and p53-mediated transcriptional reprogramming, have been shown to repopulate damaged crypts after severe injury (26, 27).

These findings highlight the plasticity of the ISC compartment. Nevertheless, at sufficiently high radiation doses, endogenous regenerative capacity is inadequate to prevent lethal barrier failure. Therapeutic strategies that enhance ISC survival, promote regenerative signaling, or stabilize intestinal epithelial junctional complexes therefore represent rational mitigation approaches.

1.3 Hematopoietic Injury in Acute Radiation Syndrome

The hematopoietic compartment is similarly dependent on proliferative stem and progenitor cells and is therefore highly sensitive to radiation-induced DNA damage. Hematopoietic stem and progenitor cells (HSPC) reside within specialized bone marrow niches and give rise to all mature blood lineages. Following total body irradiation, HSCs undergo apoptosis, senescence, or functional exhaustion, leading to depletion of circulating leukocytes, erythrocytes, and platelets (3, 28, 29). Radiation-induced oxidative stress also contributes to hematopoietic injury. ROS accumulation damages mitochondrial membranes, impairs ATP production, and amplifies apoptotic signaling cascades (7, 30). Proteins that regulate mitochondrial redox homeostasis therefore influence hematopoietic radiosensitivity.

Clinically, H-ARS manifests as leukopenia, anemia, and thrombocytopenia. Leukopenia increases susceptibility to opportunistic infection, while thrombocytopenia predisposes to hemorrhagic complications (6, 7). Growth factor therapies approved for the treatment of H-ARS, such as filgrastim and pegfilgrastim, stimulate granulopoiesis and improve survival in preclinical and clinical contexts (13, 31). However, these interventions do not directly address gastrointestinal injury and may not provide sufficient protection at radiation doses that induce overlapping gastrointestinal damage.

Because high-dose radiation frequently induces concurrent hematopoietic and gastrointestinal injury, targeting signaling pathways that enhance resilience across multiple tissues may offer broader therapeutic benefit.

1.4 Pro-survival signaling pathways in radiation response

Ionizing radiation initiates a highly coordinated cellular stress response that extends beyond direct DNA damage. While the DDR orchestrates repair and checkpoint activation through ATM, ATR, and p53 signaling (4, 5), cell fate following irradiation is ultimately determined by the integration of pro-apoptotic and pro-survival signaling cascades. Among these, the mitogen-activated protein kinase (MAPK) pathway and the phosphoinositide 3-kinase (PI3K)/Akt pathway are central regulators of radiation response (32-35).

The MAPK family includes ERK1/2, c-Jun N-terminal kinase (JNK), and p38 kinases, each of which can be activated by radiation exposure (32). JNK and p38 are frequently associated with stress-induced apoptosis and inflammatory signaling, whereas ERK1/2 activation is more commonly linked to proliferation and survival responses (32, 33). However, the functional consequences of ERK activation are highly context-dependent and influenced by the magnitude, duration, and timing of phosphorylation.

ERK signaling exhibits temporal dynamics that critically influence downstream transcriptional programs. Sustained ERK activation has been associated with induction of cytoprotective genes, promotion of cell cycle re-entry, and enhancement of clonogenic survival following genotoxic stress (32, 36). In contrast, transient or dysregulated ERK activation may be insufficient to prevent apoptotic progression (33). The mechanisms governing these kinetic patterns involve feedback regulation through dual-specificity phosphatases, protein phosphatase 2A (PP2A), and scaffold proteins that spatially constrain signaling complexes (33, 37-39).

Parallel to MAPK signaling, the PI3K/Akt pathway promotes survival through phosphorylation of pro-apoptotic proteins such as BAD, modulation of FOXO transcription factors, and activation of mTOR-dependent anabolic pathways (34, 35, 40). Akt activation also intersects with DNA repair machinery, influencing homologous recombination and non-homologous end joining processes (41, 42). Furthermore, Akt

signaling contributes to stabilization of mitochondrial membranes, limiting cytochrome c release and downstream caspase activation (43).

Radiation-induced ROS accumulation disrupts mitochondrial membrane potential, oxidizes lipids and proteins, and amplifies apoptotic signaling (44). The balance between mitochondrial injury and survival signaling determines whether irradiated cells undergo apoptosis, senescence, or functional recovery (7, 30). Importantly, signaling pathways activated at the plasma membrane—including those mediated by G protein–coupled receptors—can modulate these intracellular stress responses.

Thus, modulation of pro-survival signaling kinetics, rather than direct interference with DNA damage itself, represents a biologically plausible strategy for mitigating radiation-induced injury. Therapeutic interventions that sustain adaptive ERK and Akt signaling during critical post-irradiation windows may enhance tissue resilience and improve survival outcomes.

1.5 Lysophosphatidic acid receptor 2 as a therapeutic target

Lysophosphatidic acid (LPA) is a bioactive lipid mediator produced by autotaxin-mediated hydrolysis of lysophosphatidylcholine. LPA signals through six G protein–coupled receptors (LPAR1–6), which couple to multiple G proteins and activate diverse downstream pathways (45). Among these receptors, LPAR2 has been implicated in radiation mitigation. LPAR2 expression is upregulated following γ-irradiation through ATM-dependent NF-κB activation, suggesting integration within the DNA damage response (36). Activation of LPAR2 promotes assembly of multiprotein signaling complexes involving TRIP6 and NHERF2, leading to activation of ERK1/2 and Akt pathways (46-50).

Beyond kinase activation, LPAR2 directly interacts with the pro-apoptotic protein Siva-1, facilitating its proteasomal degradation and thereby attenuating mitochondrial apoptosis (43, 51). LPAR2 activation has also been shown to accelerate clearance of γH2AX foci, consistent with enhanced resolution of DNA damage (36, 52). In intestinal models, LPAR2 stimulation reduces radiation-induced disruption of tight junction proteins and preserves barrier function (53).

While LPAR stimulation provides an attractive physiological target for radiation mitigation, LPA itself is not suitable for use as a pharmacologic agent due to rapid metabolism, short plasma half-life, and structural instability (54). Research over the past twenty years has focused on the potential of LPAR2 agonists to mitigate radiation damage. Starting with the stable, synthetic lipid-like LPA mimic known as octadecenyl thiophosphate (OTP), we refined multiple non-lipid benzoic acid derivatives through high-throughput screening campaigns and medicinal chemistry to identify Radioprotectin-1 (RP-1), a third-generation LPAR2-specific agonist with 6 pM potency at the human receptor (**Figure 1)** (49, 50, 55). RP-1 has been shown to improve γ-H2AX foci resolution, trigger prolonged Akt and ERK signaling, and decrease apoptosis (56). Furthermore, it protects Lgr5-positive intestinal stem cells in small intestinal enteroid models and improved survival by 50% in mice in a GI-ARS model (56). These findings provide a mechanistically grounded basis for therapeutic targeting of LPAR2 in ARS.

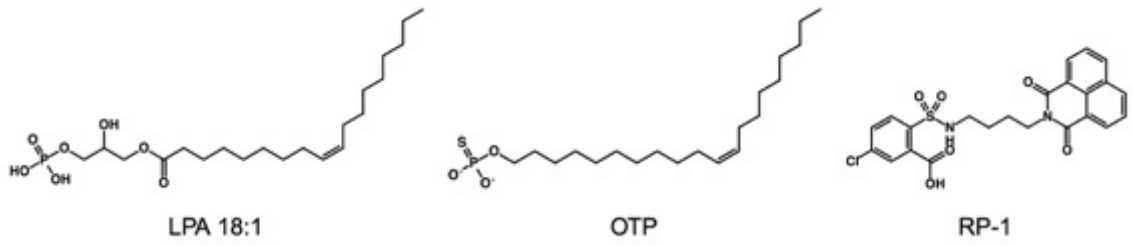

Figure 1. **LPAR agonists.** Structural comparison of LPAR agonists LPA 18:1, OTP, and RP-1. Created in BioRender. Derek D, N. (2026) https://BioRender.com/ iz6qbsa. Figure adapted from the author's original publication (57).

1.6 Pharmacokinetic optimization and extended-release formulation

Although RP-1 demonstrated mitigation efficacy in murine models of GI-ARS, its initial aqueous (AQ) formulation exhibited pharmacokinetic (PK) properties that limited translational practicality (56). Specifically, the AQ formulation was characterized by relatively rapid plasma clearance and short mean plasma residence time, necessitating twice-daily subcutaneous administration for three consecutive days

beginning 24 hours post-irradiation to achieve survival benefit. While effective under controlled laboratory conditions, such a dosing schedule may be difficult to implement in large-scale radiation emergency scenarios.

Development of medical radiation countermeasures requires consideration not only of biological efficacy but also of feasibility in mass casualty settings (12, 58). Simplified dosing regimens, prolonged therapeutic exposure, and predictable pharmacokinetics are critical factors for field deployment. In the context of GI-ARS, the timing of epithelial stem cell loss and maximal crypt depletion occurs within several days following irradiation (17-19), suggesting that sustained receptor engagement during this window may be advantageous.

To address these limitations, a multilayered water-in-oil-in-water (W/O/W) microemulsion (ME) delivery system was developed (59-61). Microemulsions are thermodynamically stable dispersions of oil and water stabilized by surfactants, capable of encapsulating small molecules and modulating release kinetics (62, 63). The W/O/W architecture enables biphasic drug release: an initial burst from the external AQ phase followed by sustained release from an internal AQ reservoir dispersed within the oil layer (**Figure 2** and **Table 1**) (60, 61). This configuration is designed to prolong systemic exposure while reducing dosing frequency.

Extended-release formulations may offer biological advantages beyond logistical convenience. Sustained systemic levels of RP-1 could maintain activation of LPAR2-mediated ERK and Akt signaling during the critical period of post-irradiation intestinal epithelial vulnerability. In addition, predictable PK in both murine and non-human primate models support translational scalability and dose extrapolation. Thus, PK optimization represents a central step in advancing RP-1 from proof-of-concept mitigation toward practical application as a radiation medical countermeasure.

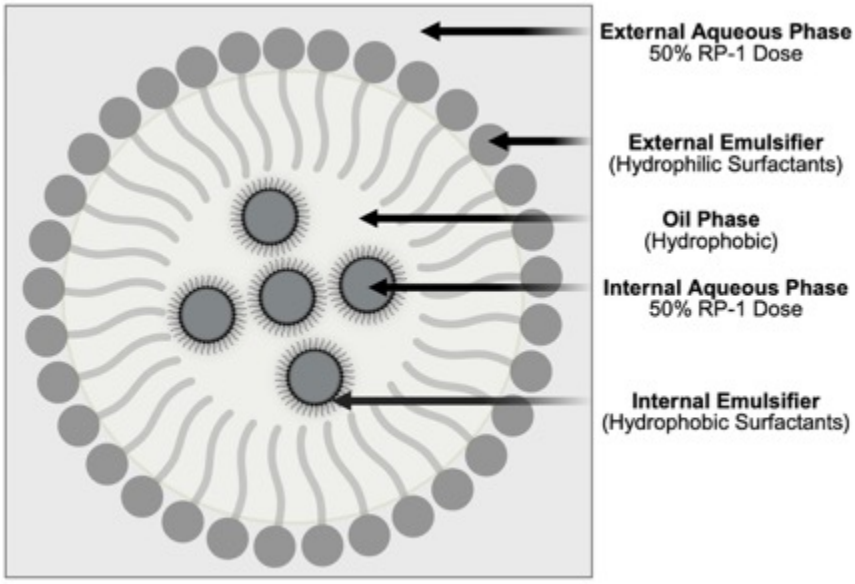

Figure 2. **RP-1 W/O/W microemulsion provides two pools of drug for delivery.** By loading the overall dose of RP-1 ratiometrically between an internal AQ phase encapsulated in hydrophobic oil which is further emulsified with hydrophilic surfactants within an external AQ phase, a multilayered W/O/W ME delivery system is achieved. With this formulation, 50% of total RP-1 is administered in a burst release via the external AW phase, while 50% is slowly released to maintain plasma concentration over an extended period from the internal AQ phase. Created in BioRender. Derek D, N. (2025) https://BioRender.com/i7hh7nb. Figure adapted from the author's original publication (57).

1.7 Immediate early response gene X-1 (IEX-1) in tissue radiosensitivity

Immediate early response gene IEX-1, also known as IER3, was initially identified as a transcript rapidly induced following exposure to ionizing radiation (64). As an immediate early gene, IEX-1 is transcriptionally upregulated without requiring new protein synthesis, positioning it as an early mediator of stress adaptation. Its expression can be induced by diverse stimuli including oxidative stress, inflammatory cytokines, and genotoxic injury through pathways involving p53, NF-κB, and ERK signaling (37, 64-66).

IEX-1 functions as a stress-responsive adaptor protein, and in some cases as transcriptional regulator (67, 68). One of its best-characterized roles involves regulation of mitochondrial redox homeostasis. IEX-1 interacts with the F1Fo-ATP synthase inhibitor protein (IF1), promoting IF1 degradation and enhancing ATP synthase activity (44). Through this mechanism, IEX-1 limits excessive mitochondrial ROS accumulation

during stress. Because radiation exposure generates substantial oxidative stress and mitochondrial dysfunction, proteins that regulate ROS accumulation may significantly influence cellular radiosensitivity.

In addition to its mitochondrial role, IEX-1 participates in regulation of stress-response kinase signaling. ERK-mediated phosphorylation stabilizes IEX-1 protein, while IEX-1 in turn modulates ERK dephosphorylation through interactions with B56-containing PP2A phosphatase complexes (38, 39, 66). This reciprocal relationship suggests that IEX-1 functions within a feedback loop that influences the amplitude and duration of ERK activation. Because ERK signaling kinetics are known to determine downstream cell fate following genotoxic stress (33, 34), disruption of IEX-1 may alter the temporal coordination of pro-survival signaling following radiation.

Beyond ERK, IEX-1 has been reported to interact with apoptosis-regulatory proteins including CAML, TRAIL, MCL1, and BAT3, indicating broader integration within stress signaling networks (67). In hematopoietic cells, IEX-1 deficiency has been associated with impaired erythroid recovery, thrombocytopenia, increased ROS accumulation in hematopoietic stem cells, and heightened susceptibility to radiation-induced apoptosis (5, 37). These findings support a role for IEX-1 in maintaining hematopoietic resilience under conditions of genotoxic stress.

However, comparatively little is known about the contribution of IEX-1 to gastrointestinal radiation injury. The intestinal epithelium is highly dependent on coordinated regulation of proliferation, differentiation, and apoptosis, processes that intersect with ERK signaling and mitochondrial function. Whether IEX-1 influences intestinal radiosensitivity, and how its stress-responsive functions integrate with receptor-mediated pro-survival signaling pathways, remains undefined. Taken together, existing literature supports the concept that IEX-1 may serve as a regulator of tissue responses to radiation-induced stress. Clarifying its role within the context of ARS—especially GI-ARS—may provide insight into signaling networks that influence organism-level survival following irradiation.

1.8 Knowledge gap and rationale

Collectively, prior investigations establish that activation of LPAR2 promotes pro-survival signaling and mitigates radiation-induced gastrointestinal injury in

preclinical models (43, 50, 56, 69). Pharmacologic stimulation of this receptor enhances ERK and Akt activation, reduces apoptotic signaling, and preserves intestinal crypt architecture when administered following irradiation (36, 50). These findings provide a mechanistic foundation for targeting lipid-mediated signaling pathways in the development of radiation medical countermeasures.

However, several critical gaps remain. First, although RP-1 has demonstrated mitigation efficacy in murine models, its initial aqueous formulation exhibits pharmacokinetic limitations that constrain translational applicability (56). Rapid clearance and short systemic exposure necessitate repeated dosing, which may be impractical in large-scale radiation emergencies. Whether pharmacokinetic optimization through extended-release formulation can maintain biological efficacy while simplifying administration regimens requires systematic evaluation.

Second, while LPAR2 activation is known to engage ERK-dependent pro-survival pathways, the downstream molecular mediators that integrate receptor activation with coordinated stress response remain incompletely characterized. Sustained ERK signaling, extending beyond 16 h of a single administration of LPA, has been associated with enhanced survival following genotoxic stress (32, 36), yet the regulatory mechanisms governing ERK signaling kinetics in irradiated tissues are not fully defined.

Third, although IEX-1 has been implicated in hematopoietic stress responses and mitochondrial redox regulation (5, 37, 65) its role in gastrointestinal radiosensitivity and its potential integration with lipid-mediated signaling pathways have not been fully examined. Given its established functions in ERK modulation and oxidative stress control, IEX-1 represents a plausible regulator of tissue resilience following irradiation.
Accordingly, there exists a translational and mechanistic need to:

1. Optimize LPAR2 agonist pharmacokinetics to improve feasibility for post-exposure mitigation.
2. Evaluate the biological impact of sustained receptor activation in models of acute radiation syndrome.
3. Clarify the contribution of IEX-1 to tissue radiosensitivity and its relationship to pro-survival signaling dynamics.

Addressing these questions requires an integrated approach that combines formulation development, preclinical efficacy assessment, and mechanistic investigation. By pursuing this strategy, the present thesis seeks to advance LPAR2 activation from experimental proof-of-concept toward practical radiation medical countermeasure development, while simultaneously improving understanding of stress-responsive signaling networks that influence radiation resilience.

2. Objectives

The central hypothesis of this thesis is that pharmacologic activation of LPAR2 can be translationally optimized through extended-release formulation to provide effective post-exposure mitigation of ARS, and that modulation of stress-responsive signaling pathways—including those involving ERK and IEX-1—contributes to tissue radiosensitivity and survival outcomes. The overall aim of this work was to advance LPAR2 activation as a practical radiation medical countermeasure while examining the contribution of IEX-1 to tissue resilience in models of ARS.

2.1 To optimize the pharmacokinetic profile of the LPAR2 agonist RP-1 through development of an extended-release ME formulation

This objective addressed the translational limitation of the aqueous RP-1 formulation. Specific goals included:

- Development of a multilayered W/O/W ME delivery system.
- Comparative pharmacokinetic analysis of AQ and ME formulations in murine and NHP models.

This objective directly addressed the need for simplified dosing and sustained systemic exposure suitable for post-exposure mitigation scenarios.

2.2 To evaluate whether extended-release RP-1 administration improves survival outcomes and preserves intestinal integrity in a murine model of GI-ARS

This objective focused on preclinical efficacy and translational relevance. Specific goals included:

- Determination of 21-day survival following high-dose irradiation with RP-1 ME administered beginning 24 h post-exposure.
- Comparison of dosing frequency relative to the AQ formulation.
- Quantification of total and regenerating intestinal crypts at the post-irradiation nadir.

This objective examined whether pharmacokinetic optimization translated into therapeutically relevant biological and organism-level benefit.

2.3 To characterize the impact of LPAR2 activation on pro-survival signaling pathways following irradiation.

This objective provided mechanistic context for mitigation effects. Specific goals included:

- Assessment of ERK1/2 and Akt phosphorylation kinetics following irradiation and RP-1 treatment.
- Evaluation of sustained signaling patterns consistent with enhanced cellular resilience.
- Measurement of caspase-mediated apoptotic signaling.

This objective was designed to evaluate signaling dynamics without presuming direct causal relationships between pathway activation and survival outcomes.

2.4 To determine the contribution of IEX-1 to hematopoietic and gastrointestinal radiosensitivity and to explore the relationship to stress-response signaling pathways.

This objective addressed the mechanistic gap identified in section 1.8. Specific goals included:

- Comparison of survival outcomes in wild-type (WT) and IEX-1-deficient mice in models of H- and GI-ARS.
- Evaluation of intestinal regenerative capacity in *in vitro* enteroid systems.
- Assessment of ERK1/2 phosphorylation dynamics in the presence and absence of IEX-1.

This objective sought to clarify whether IEX-1 functions as a determinant of tissue radiosensitivity and to explore its potential integration within receptor-mediated pro-survival signaling networks.

3. Methods

3.1 Animal models, husbandry, and ethical compliance

All animal experiments were conducted in accordance with institutional and federal regulations governing the ethical use of vertebrate animals in research. Murine protocols were reviewed and approved by the Institutional Animal Care and Use Committee (IACUC) of the University of Tennessee Health Science Center. All procedures involving NHP were approved by the University of Maryland School of Medicine IACUC.

3.1.1 Wild-type murine cohorts

Specific pathogen-free C57BL/6J mice were obtained from The Jackson Laboratory (Bar Harbor, ME, USA) and housed in the UTHSC Regional Biocontainment Laboratory in ventilated Allentown biocontainment cages. Male and female cohorts were maintained separately and experiments involving each sex were conducted independently to minimize potential pheromone-associated physiological effects. Mice were 10–12 weeks of age upon arrival and were allowed to acclimate for one week prior to initiation of experimental procedures.

Animals were maintained on sterilized Teklad 7912 rodent chow (Inotiv, Indianapolis, IN, USA) with unrestricted access to autoclaved water. Health assessments were performed daily under baseline conditions and increased to twice daily during the anticipated period of radiation injury progression. Predefined humane endpoint criteria were established in accordance with IACUC-approved scoring systems and included severe lethargy, inability to ambulate, respiratory distress, cyanosis, abdominal distension, persistent ataxia, unresponsiveness, facial swelling, head tilt, or open wounds. Animals meeting these criteria were euthanized promptly to minimize distress. Supportive nutritional supplementation in the form of sterilized DietGel 76A (ClearH_2O, Westbrook, ME, USA) was provided ad libitum beginning on day 4 following irradiation to support hydration and caloric intake during the expected crypt nadir period.

3.1.2 IEX-1 knockout model

To investigate the contribution of IEX-1 to radiation response, B6;129X1-*Ier3*^{tm1Raku}/J mice (IEX-1 knockout [KO], stock #012664) (70) were obtained from The Jackson Laboratory (Bar Harbor, MI, USA) and bred in-house under specific pathogen-free conditions. Genotyping was performed using PCR analysis of genomic DNA extracted from tail biopsies. Amplification employed the following established primer sequences: #11229 5'-CGCCTACATTTTGCTTCCTC-3', #11230 5'-GAGGGTAGAGCACCCT-TCG-3', and mutant-specific primer oIMR7266 5'-GTGGGCTCTATGGCTTCTGA-3'. WT littermates served as experimental controls. Female mice 8-14 weeks of age at time of experiments. Animals were randomized to treatment groups prior to irradiation.

3.1.3 Non-human primate cohort

For pharmacokinetic evaluation in a higher-order species, a cohort of seven rhesus macaques (six male and one female) was housed individually in stainless steel enclosures. Animals were maintained on a Global 20% Protein Primate Diet supplemented with fresh fruit and commercial primate enrichment treats. Reverse osmosis–purified water was provided continuously via sipper lines and in-cage bottles. Daily veterinary assessments were conducted to monitor social interaction, activity level, and clinical condition.

3.2 Irradiation procedures and dosimetry

All irradiations were performed using a ^{137}Cs source JL Shepherd Mark I γ-irradiator operating at a dose rate below 1 Gy per minute. Dosimetric calibration was verified using thermoluminescent dosimeters incorporated into each irradiation session. Independent dose verification was performed by MD Anderson Cancer Center Radiation Dosimetry Services (Houston, TX) to ensure accuracy and reproducibility.

3.2.1 Total body irradiation (TBI)

For H-ARS studies, mice were subjected to 9 Gy TBI, corresponding to an $LD_{70/30}$ model as described in our previous work (49, 52, 56). Animals were placed in

well-ventilated restrainers to ensure uniform radiation exposure. Following irradiation, mice were returned to clean cages and monitored daily for 30 days for survival analysis.

For studies assessing the effect of irradiation on systemic drug pharmacokinetics, mice were exposed to 16 Gy TBI. RP-1 was administered intravenously (IV) via tail vein injection 24 h following irradiation to evaluate post-exposure pharmacokinetics.

3.2.2 Partial body irradiation with 5% bone marrow shielding (PBI-BM5)

To model GI-ARS while preserving limited hematopoietic function, partial body irradiation with approximately 5% bone marrow shielding was performed as described in our previous work (49, 52, 56). Bilateral lower femurs, tibiae, fibulae, and paws were protected using custom-fabricated lead shields, thereby sparing a defined fraction of total bone marrow mass. Mice were anesthetized by intraperitoneal (IP) injection of ketamine (87 mg/kg) and xylazine (13 mg/kg) prior to irradiation to minimize movement and ensure consistent shielding geometry. The remainder of the body was exposed to 16.0–16.5 Gy, corresponding to an $LD_{70/21}$ gastrointestinal injury model. RP-1 ME was administered in 0.1 ml (female) or 0.05 ml (male) dose volumes by subcutaneous (SC) injection starting 24 h post-irradiation. Subjects were monitored twice daily for 21 days, and any mice exhibiting clinical signs consistent with severe gastrointestinal radiation injury were euthanized in accordance with humane endpoint criteria.

3.3 RP-1 formulation development and administration

RP-1 was synthesized through medicinal chemistry collaboration and prepared under sterile conditions for *in vivo* administration. All formulations were prepared fresh prior to injection unless otherwise indicated.

3.3.1 Aqueous formulation

The AQ formulation of RP-1 used for pharmacokinetic analyses was prepared in a vehicle consisting of phosphate-buffered saline (PBS) supplemented with 1% (v/v) ethanol and 2% (v/v) 1,2-propanediol to facilitate solubilization. SC administration was performed in the dorsal cervical region.

3.3.2 Development of extended-release microemulsion formulation

To prolong systemic exposure and reduce dosing frequency, a multilayered water-W/O/W ME delivery system was developed by modification of a previously published formulation (59-61). The preparation began with the creation of a primary W/O ME containing half of the total RP-1 in its internal AQ phase. This primary system was optimized via a pseudo-ternary phase diagram using the water titration technique, utilizing Labrafac Lipophile WL1349 oil (Gattefossé, Paramus, NJ, USA), a 1:1 blend of surfactants Capryol 90 (Gattefossé, Paramus, NJ, USA) and soybean L-α-lecithin (Calbiochem, Billerica, MA), and water in a 3:5:2 ratio. Separately, an external AQ phase was formulated with the remaining RP-1, consisting of water, a 1:1 mixture of Labrasol (Gattefossé, Paramus, NJ, USA) and Cremophor EL (Sigma-Aldrich, St. Louis, MO, USA), and the co-solvent propylene glycol (Thermo Fisher Scientific, Waltham, MA, USA) in a 5:2:3 ratio (**Table 1**). Finally, the primary ME was emulsified into the external phase with the specific incorporation ratio determined by previously established titration methods (59, 61).

The architecture of the W/O/W system was designed such that approximately half of the administered RP-1 dose was available for immediate systemic absorption from the external aqueous phase, while the remaining fraction was retained within the internal reservoir and released gradually over time. SC injection volumes were standardized to 0.1 mL for female mice and 0.05 mL for male mice.

Table 1. RP-1 W/O/W Microemulsion Components

Internal W/O ME	% of Phase	External AQ Phase	% of Phase
Labrafac Lipophile WL 1349	30%	Labrasol	10%
Capryol 90	25%	Cremophor EL	10%
Soybean L-α-Lecithin	25%	Propylene Glycol	30%
Water for Injection	20%	Water for Injection	50%

Ratio of internal W/O microemulsion incorporated into the final multilayered microemulsion determined by titration method.

3.3.3 Dosing paradigms in GI-ARS studies

For evaluation of mitigation efficacy in the gastrointestinal acute radiation syndrome model, RP-1 microemulsion was administered beginning 24 h following partial body irradiation with bone marrow shielding. The primary dosing paradigm

consisted of two subcutaneous injections administered at 24 h and 72 h post-irradiation. Exploratory dosing schedules included a single administration at 24 h and delayed administration at 48 and 96 h post-irradiation to evaluate the impact of timing on survival outcomes. In male cohorts, dose-response evaluation was conducted due to observed differences in tolerability at higher doses. Animals were monitored closely following injection for evidence of local irritation or systemic adverse effects.

3.4 Pharmacokinetic studies

Pharmacokinetic studies were conducted to characterize systemic exposure, clearance, and residence time of RP-1 following intravenous and subcutaneous administration in mice and non-human primates (NHP). In addition, the potential impact of radiation exposure and sex-dependent variability on drug disposition was evaluated in mice.

3.4.1 Plasma preparation

For murine pharmacokinetic studies, blood samples were collected from 4-6 mice of both sexes from the inferior vena cava at predetermined time points following RP-1 administration. For IV pharmacokinetic assessment, RP-1 was delivered via tail vein injection with sample collection at 10 min, 30 min, 1 h, and 6 h post-injection. For SC pharmacokinetic assessment, RP-1 administration was performed in the dorsal cervical region with sample collection at 30 min, 1 h, 2 h, 6 h, 24 h, 48 h, and 72 h post-injection. To assess translational scalability, plasma samples were generated from a cohort of 6 male and 1 female rhesus macaques receiving abdominal SC administration of RP-1. Serial blood sampling was performed according to approved veterinary protocols at 30 min, 1 h, 2 h, 4 h, 6 h, 8 h, 24 h, 48 h, and 72 h post-injection. From both species, blood was also collected from untreated animals for blank plasma preparation. Whole blood was collected into K_3-EDTA-coated Sarstedt Microvette 500 K3E tubes (Sarstedt, Newton, NC, USA). Plasma was generated by centrifugation at 5,000 RPM for 5 min and was stored immediately at -80°C prior to analysis.

3.4.2 Quantification of plasma RP-1 by LC-MS/MS

Calibration standards were prepared by diluting RP-1 into pooled blank K_3-EDTA plasma over a concentration range of 0–1000 ng/mL. A structurally related analog, 2-[4-(1,3-dioxo-1H,3H-benzoisoquinolin-2-yl)butylsulfamoyl]benzoic acid (DBIBB), was used as an internal standard (IS) and added to all samples at a final concentration of 50 ng/mL prior to extraction. RP-1 and internal standard were extracted from plasma using a liquid–liquid extraction method. Briefly, 150 µL of water-saturated butanol was added to 50 µL plasma samples containing internal standard. Samples were vortexed vigorously for 5 min to facilitate analyte partitioning into the organic phase and subsequently centrifuged at 15,000 rpm for 5 min to achieve phase separation. The upper organic layer was collected, evaporated to dryness, and reconstituted in LC–MS grade methanol prior to analysis.

Chromatographic separation was performed using a Shimadzu Prominence Series LC system equipped with LC-20AD pumps, a Nexera autosampler, and a CTO-20 AC column oven (Shimadzu Scientific Instruments, Columbia, MD, USA). Analytes were resolved on a Gemini C18 reversed-phase column (50 × 2.0 mm, 5 µm particle size, 110 Å pore size; Phenomenex, Torrance, CA, USA) maintained at 35°C with an injection volume of 20 µL. Mobile phase A consisted of 0.1% (v/v) trifluoroacetic acid (TFA) in LC–MS grade water, and mobile phase B consisted of 0.1% (v/v) TFA in LC–MS grade acetonitrile. A 5-minute gradient was applied, beginning at 10% mobile phase B, increasing to 35% at 1 minute, ramping to 95% at 4.1 minutes, held at 95% for 1 minute, and then returning to 10% for re-equilibration.

Mass spectrometric detection was performed using an AB Sciex 4500 QTRAP triple quadrupole linear ion trap mass spectrometer equipped with a Turbo V ion spray source operating in positive electrospray ionization mode (Applied Biosystems Sciex LLC, Marlborough, MA). Quantification was conducted in multiple reaction monitoring (MRM) mode with the transition of the *m/z* 487.2 parent ion to the *m/z* 252.2 daughter ion for RP-1 and the transition of the *m/z* 453.2 parent ion to the *m/z* 252.2 daughter ion for IS.

Quadrupoles Q1 and Q3 were operated at unit resolution. Data acquisition and peak integration were performed using AB Sciex Analyst software (version 1.6.1). Peak area ratios of RP-1 to internal standard were calculated for each sample. Concentrations

were interpolated from calibration curves generated using linear regression of peak area ratios versus nominal concentrations. To account for minor variations in dosing due to average cohort weight–based injection volumes, measured plasma concentrations in murine studies were normalized to the intended 3 mg/kg target dose based on individual animal body weight at the time of administration.

3.4.3 Pharmacokinetic modeling and analysis

Pharmacokinetic parameters were determined using non-compartmental analysis (NCA) of plasma concentration–time data using Phoenix WinNonlin 8.4.0 (Certara USA, Inc., Princeton, NJ, USA). The extravascular model was applied for the SC data, and the IV bolus model was applied for the IV data. The "linear-up log-down" method was used to estimate the area under the C_t curve (AUC) values. The terminal phase was defined as at least three time points at the end of the C_t profile, and the elimination rate constant (K_{el}) was estimated using an unweighted log-linear regression of the terminal phase. The terminal elimination half-life ($t_{1/2}$) was estimated as $0.693/K_{el}$. Other parameters estimated included time to reach C_{max} (T_{max}), mean residence time (MRT), bioavailability (F), and total body clearance (CL_T = Dose/AUC).

Comparative analyses were performed between AQ and ME formulations to evaluate differences in systemic exposure and clearance kinetics. Additional analyses were conducted to assess the impact of radiation exposure on pharmacokinetic behavior and to evaluate sex-dependent variability in murine cohorts. NHP pharmacokinetic parameters were calculated using the same analytical approach to enable interspecies comparison of systemic exposure and elimination characteristics.

3.5 Gastrointestinal injury assessment

Evaluation of gastrointestinal radiation injury included organism-level survival analysis and tissue-level assessment of crypt survival and regenerative capacity. Experiments were performed in the PBI-BM5 model to isolate gastrointestinal injury while preserving limited hematopoietic function.

3.5.1 Survival analysis

Following PBI-BM5 exposure (16.0–16.5 Gy), mice were returned to sterile housing, and RP-1 ME was administered SC beginning 24 h after irradiation in accordance with radiation mitigator criteria. In the primary mitigation paradigm, a second dose was administered at 72 h post-irradiation. Control animals received vehicle injections under identical conditions. Animals were observed daily over a 21-day period for morbidity and mortality. Predefined humane endpoints were applied consistently across treatment groups. Animals meeting endpoint criteria were euthanized and recorded as non-survivors for Kaplan-Meier analysis. Survival curves were generated for each treatment group over the observation period. Differences in survival distributions were evaluated using the Mantel-Cox log-rank test.

3.5.2 Intestinal crypt microcolony assay

To assess structural preservation and regenerative capacity of the intestinal epithelium, mice were euthanized on post-irradiation day 5, corresponding to the expected nadir of crypt depletion in the GI-ARS model. Segments of jejunum were harvested at standardized anatomical locations to ensure reproducibility across animals—specifically, at 9 cm, 11 cm, and 13 cm distal to the stomach to minimize regional variability in crypt density. Excised intestinal segments were flushed with cold PBS to remove luminal contents and fixed in neutral-buffered formalin. Following fixation, tissues were processed through graded alcohol dehydration, paraffin embedded, and sectioned at 5 μm thickness.

For morphological evaluation and crypt survival quantification, sections were stained with hematoxylin and eosin (H&E). Surviving crypts were identified using the established microcolony assay criterion, defined as a crypt containing at least ten adjacent viable epithelial cells as described previously (50, 71). Only well-oriented cross-sections were included in analysis to ensure accurate circumferential crypt counting.

To assess proliferative activity within regenerating crypts, adjacent sections were subjected to immunohistochemical staining for Ki67 as described previously (72). Following deparaffinization and rehydration, heat-mediated antigen retrieval was

performed. Endogenous peroxidase activity was blocked prior to incubation with primary anti-Ki67 antibody. Sections were subsequently incubated with appropriate secondary antibody conjugates and visualized using chromogenic substrate development. Slides were counterstained with hematoxylin.

For each animal, multiple circumferential sections were evaluated. Total surviving crypts and Ki67-positive crypts were counted under light microscopy. All histological assessments were performed independently by two investigators blinded to treatment allocation to minimize observational bias. Average crypt counts per animal were calculated and used for group comparisons using unpaired t-test.

3.6 Cell culture models

3.6.1 Mouse embryonic fibroblast culture

Mouse embryonic fibroblasts (MEF) were generated from LPAR1 and LPAR3 double knockout animals that endogenously express LPAR4, LPAR5, and LPAR6 at very low levels but completely lack LPAR1, LPAR2, and LPAR3. Using lentiviral overexpression, these MEFs were transduced with either empty vector (EV) or human LPAR2 to generate a stable MEF line as described previously (51). Cells were cultured at 37°C with 5% CO_2 in Dulbecco's modified Eagle medium (DMEM; Corning Inc., Corning, NY, USA) supplemented with 10% fetal bovine serum (FBS; R&D Systems, Minneapolis, MN, USA), 2 mM L-glutamine (Corning Inc., Corning, NY, USA), and 100 U/mL penicillin-streptomycin (Corning Inc., Corning, NY, USA). Cultured cells were tested regularly for mycoplasma contamination, and all experiments were performed using mycoplasma-free cells.

3.6.2 Mouse small intestinal enteroid culture

Small intestinal crypts were isolated from the jejunum and ileum of WT and IEX-1 KO mice for three-dimensional enteroid culture. Following tissue harvest, intestinal segments were flushed with cold PBS, opened longitudinally, and subjected to EDTA-based chelation with mechanical agitation to release crypt units as described previously (56, 73). Isolated crypts were embedded in growth factor–reduced Matrigel domes (Corning Inc., Corning, NJ, USA) and overlaid with IntestiCult™ Organoid

Growth Medium (OGM; STEMCELL Technologies, Vancouver, British Columbia, Canada). Approximately 350 crypts were seeded per 40 µL dome, and enteroids were maintained at 37°C in 5% CO_2 with medium replacement every two to three days. Growth kinetics, budding morphology, and structural organization were monitored microscopically over a nine-day culture period where ImageJ (v1.54) was used to measure two-dimensional area of enteroids.

3.7 Radiation and pharmacologic treatments in cell systems

For pharmacologic signaling studies, MEF were plated in triplicate wells of a 96-well plate at 1×10^4 cells per well. For caspase activation assays, cells were plated in triplicate wells of a 48-well plate at 2×10^5 cells per well. Cells were cultured in complete medium overnight, serum-deprived for 1 h, then treated with LPA 18:1 or RP-1 prior to irradiation where indicated. Irradiation (15 Gy) was delivered at a dose rate of 3.2 Gy/min to induce measurable stress signaling responses. Cells were assayed at multiple time points extending up to 16 h post-irradiation to evaluate the time-course of ERK and Akt phosphorylation dynamics as well as caspase 3/7 activation. Three to four parallel sample wells were assayed, and experiments were repeated three times.

For genetic and signaling studies, day 9 enteroid cultures derived from WT and IEX-1 KO mice were pre-treated for 2 h with LPA 18:1 or OTP prior to irradiation to 5 Gy at a dose rate of 0.6 Gy/min. Enteroids were harvested at early post-irradiation time points (1 h, 3 h, and 4 h) to assess acute ERK phosphorylation dynamics and IEX-1 expression. Three to four Matrigel domes were pooled for each sample, and Matrigel domes were mechanically disrupted in cold Cell Recovery Solution (Corning Inc., Corning, NJ, USA) as per manufacturer's instructions. Experiments were repeated three times with fresh crypt harvests from 2-3 mice.

3.8 Molecular and biochemical analyses

3.8.1 Cell-based phospho-ERK and phospho-Akt quantification

Phosphorylation of ERK1/2 and Akt in MEF was quantified using a phospho-antibody cell-based ELISA (PACE assay) as described previously (74, 75). Following treatment with LPA or RP-1 and irradiation, cells were fixed in 4% NBF, and non-

specific binding was blocked with 5% non-fat dry milk in PBS with 0.1% Triton X-100 (PBS-T). ERK and Akt phosphorylation were assayed with overnight incubation at 4°C with phospho-p44/42 MAPK (ERK1/2) antibody at 1:3000, phospho-Ser473 Akt, D9E XP antibody at 1:1000, or phospho-Thr308 Akt, 244F9 antibody at 1:1000 in 5% bovine serum albumin (BSA; Sigma-Aldrich, St. Louis, MO, USA). For normalization, total ERK1/2 and total Akt were assessed with the corresponding antibodies in 5% non-fat dry milk at 1:1000. All primary antibodies were from Cell Signaling Technology, Inc. (Danvers, MA, USA). Plates were incubated for 1 h at room temperature with horseradish peroxidase coupled goat anti-rabbit IgG secondary antibody (Thermo Fisher Scientific, Waltham, MA, USA) at 1:1000 in 5% non-fat dry milk. Thermo Ultra-TMB ELISA Substrate (Thermo Fisher Scientific, Waltham, MA, USA) was used to visualize HRP signal, and the signal development was then stopped with 2 M sulfuric acid. Absorbance was read immediately at 450 nm using a FlexStation 3 (Molecular Devices, San Jose, CA, USA). Data were background-corrected, and phosphorylated signal was normalized to total protein level. Fold-change in ERK or Akt phosphorylation was calculated vs vehicle control, and differences in activation magnitude and duration under various treatment conditions were evaluated.

3.8.2 Caspase 3/7 activity assay

Apoptotic activity following irradiation and LPAR stimulation was quantified using a luminescence-based Caspase-Glo® 3/7 assay (Promega, Madison, WI) according to the manufacturer's protocol. Following treatment with RP-1 and irradiation, Caspase-Glo® 3/7 reagent was added directly to culture wells in a 1:4 ratio with existing medium. Plates were gently mixed to ensure uniform distribution and incubated at room temperature for 30 min to allow complete cell lysis and substrate cleavage. 200 µL of each lysate were then transferred to a 96-well, white-walled assay plate. Luminescence was measured over 1000 ms integration using a FlexStation 3 multi-mode microplate reader. Background luminescence from reagent-only wells was subtracted from all readings. Caspase activity values were normalized to non-irradiated vehicle-treated controls, and fold change in caspase 3/7 activation was determined.

3.8.3 Immunoblot analysis of ERK phosphorylation in enteroids

Protein lysates were prepared from pooled enteroid cultures by lysis in M-PER™ buffer containing protease and phosphatase inhibitors (Thermo Fisher Scientific, Waltham, MA, USA). Protein concentration was determined using Pierce™ BCA protein assay kit (Thermo Fisher Scientific, Waltham, MA, USA). A total of 15 μg protein was separated by 12% SDS-PAGE and transferred to nitrocellulose membranes. Membranes were blocked with 5% non-fat milk in TRIS-buffered saline with 0.05% Tween 20 (TBS-T), then incubated with rabbit anti-phospho-ERK1/2 primary antibody at 1:1000 dilution, washed, and incubated with secondary goat anti-rabbit IgG HRP antibodies at 1:3000 dilution. Protein was visualized using the Super Signal™ West Pico PLUS Chemiluminescent Substrate kit (Thermo Fisher Scientific, Waltham, MA, USA). For normalization, membranes were stripped using Restore™ Western Blot Stripping Buffer (Thermo Fisher Scientific, Waltham, MA, UDA) and re-probed with rabbit anti-total ERK1/2 at 1:1000 dilution. Chemiluminescent signal was visualized using a Bio-Rad ChemiDoc™ XRS system, and densitometric analyses were conducted in the Bio-Rad Image Lab 5.2.1 software (Bio-Rad, Hercules, CA, USA).

3.8.4 Quantitative RT-PCR

For *in vivo* studies, WT mice were pre-treated with OTP 30 min prior to 9 Gy TBI or 16 Gy PBI-BM5. Whole blood and intestinal mucosa were harvested 3 h post-irradiation. Enteroid RNA was also isolated from pooled domes pre-treated with LPA or OTP 2 h prior to exposure to 5 Gy irradiation. Total RNA was extracted using RNeasy Protect Animal Blood Kit, RNeasy Lipid Tissue Mini Kit, and RNeasy Micro Kit, respectively (Qiagen, Germantown, MD, USA). Equal quantities of total RNA (1 μg) from each sample were reverse transcribed into cDNA using the RevertAid Reverse Transcriptase Kit (Thermo Fisher Scientific, Waltham, MA, USA) with random hexamer primers. Reactions were performed under standardized thermal cycling conditions to ensure uniform reverse transcription efficiency across samples. RT-qPCR was performed on a QuantStudio™ 6 system using the PowerUp™ SYBR™ Mastermix (Thermo Fisher Scientific, Waltham, MA, USA) using gene-specific primers (**Table 2**). Relative gene expression was calculated using the comparative Ct (ΔΔCt) method. Target gene expression levels were normalized to endogenous housekeeping genes

Gapdh or *Rplp0* to control for variation in RNA input and reverse transcription efficiency. Fold changes were calculated relative to untreated and non-irradiated control samples.

Table 2. Primers Used in RT-qPCR

Target	Forward 5'-3'	Reverse 5'-3'
Gapdh	CTGCACCACCAACTGCTTAG	GGGCCATCCACAGTCTTCT
Rplp0	CTCTCGCTTTCTGGAGGGTG	ACGCGCTTGTACCCATTGAT
Iex-1	ATGCTACCAGCGCCGTGACA	TTAGAAGGCCGCCGGATGTTGC
Lpar1	GCTGGACCTAGCAGGCTTAC	TGCCAGGCACAAAAAGCAAT
Lpar2	TGTTCAGCCGCTCCTACTTG	AATGCCCCCAGAATGATGACA
Lpar3	GTCTTAGGCGCCTTCGTGG	TTGCACGTTACACTGCTTGC
Lpar4	GCGAGTTGCCAGTTTACACG	TTGAGTGCCCAAGAAAGAGTGT
Lpar5	TCAGCGATGAACTGTGGAAG	ACGAAGCACAGCAGGAAGAT
Lpar6	TCATCTGTGCCCTCAAAGTG	CACAGCAATGCAAACGATCT

3.9 Statistical analyses

All statistical analyses were performed using GraphPad Prism version 10.4.1 (GraphPad Software, San Diego, CA, USA). Data are presented as mean ± standard error of the mean (SEM) unless otherwise indicated. The number of biological replicates (n) is specified in the corresponding figure legends or results descriptions. Survival data were analyzed using Kaplan-Meier survival curves. Differences between survival distributions were assessed using the Mantel-Cox (log-rank) test. For comparisons between two independent groups, unpaired two-tailed Student's t-test was used. For experiments involving more than two groups or multiple time points, one-way or two-way analysis of variance (ANOVA) with Tukey's or Šídák's post hoc testing was used.

4. Results

4.1 Immediate-release RP-1 improves outcomes in GI-ARS

4.1.1 RP-1 AQ mitigates GI-ARS

To determine the effects of RP-1 in AQ formulation on radiation mitigation, survival studies were conducted in the PBI-BM5 model of GI-ARS. Female C57BL/6J mice were exposed to 16.0 Gy and treated with 0.3 mg/kg RP-1 AQ twice daily for 3 days beginning 24 h post-irradiation. Kaplan-Meier survival analysis demonstrated a substantial improvement in 21-day survival in mice treated with RP-1 AQ compared to vehicle-treated controls (**Figure 3**) (56). Statistical comparison using the Mantel-Cox log-rank test confirmed a significant 50% increase in survival in RP-1 treated mice vs vehicle control. Although radiation mitigation by RP-1 AQ was robust in the GI-ARS model, the dosing regimen required to achieve efficacy was not conducive to application as a medical countermeasure.

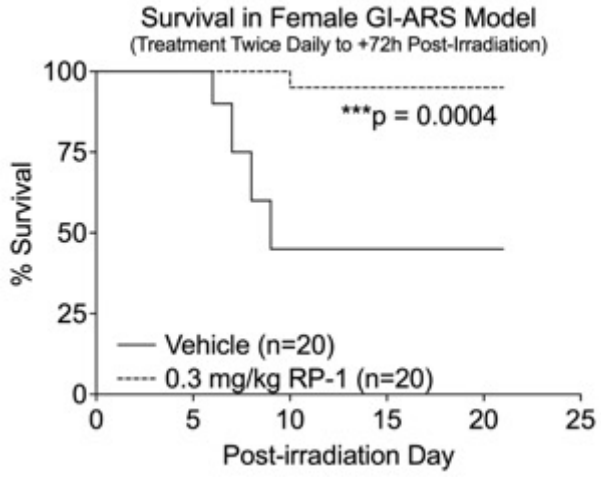

Figure 3. RP-1 AQ mitigates GI-ARS. Female mice were exposed to 16 Gy PBI-BM5 and treated with vehicle or 0.3 mg/kg RP-1 AQ twice daily for 3 days starting 24 h post-irradiation. Kaplan-Meier plots were generated for percent survival, and Mantel-Cox log-rank analysis was conducted to compare vehicle vs RP-1 AQ (n=20 per group). Figure adapted from the author's original publication (56).

4.2 Pharmacokinetic optimization of RP-1

4.2.1 RP-1 ME exhibits an extended-release pharmacokinetic profile in mice and NHP

To improve the translational feasibility of RP-1 as a radiation mitigator, a multilayered W/O/W ME formulation was developed to extend systemic exposure relative to the previously utilized AQ preparation. Pharmacokinetic characterization was performed to compare systemic drug disposition between formulations and to determine whether radiation exposure altered RP-1 pharmacokinetics. Plasma samples were collected over an extended time course to capture both early absorption and later elimination phases. Plasma concentration-time curves are presented as mean ± SEM, and unpaired t-test was used to identify differences in pharmacokinetic parameters between AQ and ME formulations.

Following administration of the AQ formulation in mice, plasma RP-1 concentrations declined rapidly, consistent with relatively short systemic persistence (**Figure 4A**). In contrast, the ME formulation produced a prolonged concentration-time profile indicative of sustained release from the internal reservoir of the ME system (**Figure 4B**). NCA performed using Phoenix WinNonlin demonstrated a marked extension in plasma half-life ($t_{½}$) with the ME formulation compared to AQ. Specifically, the mean half-life increased from approximately 1.15 h in the AQ formulation to approximately 8.42 h in the ME formulation. This increase in half-life was accompanied by increases in mean residence tie and total systemic exposure, as reflected by significantly elevated *AUC* values. Systemic plasma clearance (CL_T/F) was correspondingly reduced in the ME group (**Table 3**).

To assess translational scalability, the ME formulation was evaluated in NHP. Plasma concentration-time profiles demonstrated sustained systemic exposure following SC administration, like that observed in mice, where half-life increased from 2.11 h in the AQ formulation to 5.77 h in the ME along with corresponding increases in mean residence time and reduction systemic plasma clearance (**Figure 4C-D** and **Table 4)**. Although the sample size was limited and formal sex-stratified modeling was not feasible, NCA confirmed measurable systemic exposure and prolonged half-life consistent with extended-release behavior in this higher-order species.

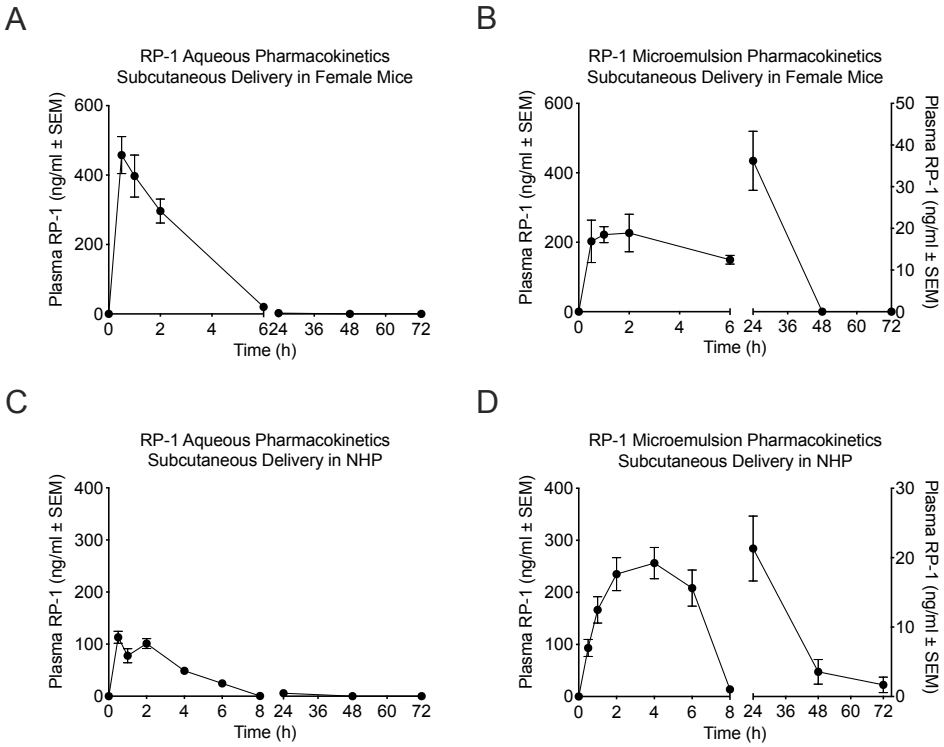

Figure 4. RP-1 ME exhibits an extended-release pharmacokinetic profile in mice and NHP. Female mice were dosed via SC injection with 3 mg/kg RP-1 in AQ (**A**) or ME formulation (**B**). Plasma samples were generated from 4-5 mice per time point. A cohort of 7 Rhesus macaques was dosed in the same paradigm (**C**-**D**) with serial blood collection and plasma generation for each animal within the cohort. RP-1 plasma concentration was quantified by LC-MS/MS, and NCA was conducted to determine pharmacokinetic parameters. Figure adapted from the author's original publication (57).

Table 3. Pharmacokinetic Parameters of RP-1 AQ vs ME Formulation in Mice

	IV	SC		
Parameter	**AQ**	**AQ**	**ME**	**p-value (AQ vs ME)**
T_{max} (h)	0	0.70 ± 0.27	1.50 ± 0.58	0.0621
$t_{1/2}$ (h)	0.32 ± 0.13	1.15 ± 0.28	8.42 ± 1.16	<0.0001 (****)
MRT (h)	0.27 ± 0.08	1.90 ± 0.13	8.58 ± 0.42	<0.0001 (****)
AUC (ng/ml*h)	1507.8 ± 415.9	1069.8 ± 166.3	2573.8 ± 479.9	0.0024 (**)
F (%)	100	71.0 ± 11.0	-	-
CL_T/F (ml/h/g)	2.05 ± 0.51	2.75 ± 0.41	1.02 ± 0.18	0.0002 (***)
CL_T (ml/h/g)	2.05 ± 0.51	1.95 ± 0.29	0.72 ± 0.12	0.0002 (***)

Table 4. Pharmacokinetic Parameters of RP-1 AQ vs ME Formulation in NHP

Parameter	SC		p-value (AQ vs ME)
	AQ	ME	
T_{max} (h)	1.00 ± 0.71	3.71± 0.76	0.0004 (***)
$t_{1/2}$ (h)	2.11 ± 0.97	5.77 ± 1.44	0.0091 (***)
MRT (h)	2.42 ± 0.17	7.87 ± 1.08	0.0029 (**)
AUC (ng/ml*h)	392.4 ± 70.6	2446.7 ± 417.8	0.0013 (**)
CL_T/F (ml/h/g)	6.67 ± 1.73	1.17 ± 0.29	0.0014 (**)

Collectively, these data demonstrate that the W/O/W ME formulation substantially prolongs systemic exposure of RP-1 compared to the AQ preparation. The extended half-life and increased residence time support reduced dosing frequency and enhance the translational applicability of RP-1 as a post-exposure radiation mitigator.

4.2.2 Sex but not irradiation affects the pharmacokinetic profile of RP-1 in mice

Previously, we have shown that the pharmacokinetic profile of OTP is not affected by sex or irradiation (49). To determine whether sex or prior radiation exposure altered systemic drug disposition, pharmacokinetic studies were conducted in irradiated and non-irradiated male and female mice. Concentration-time curves and calculated pharmacokinetic parameters were comparable within each sex regardless of irradiation, indicating that radiation exposure at the doses tested did not significantly impact RP-1 pharmacokinetics. However, noticeably less circulating RP-1 was observed in male mice, with the peak concentration at 10 min only reaching about 30% of that seen in females. This trend was consistent across non-irradiated and irradiated mice, suggesting that male mice had significantly lower drug exposure and higher plasma clearance than female mice regardless of irradiation exposure (**Figure 5** and **Table 5**). Sex-dependent pharmacokinetic modeling was not performed in full for male mice. Male cohorts were evaluated primarily for tolerability and dose-response effects, as increased sensitivity at higher doses was observed. Consequently, complete non-compartmental pharmacokinetic analysis was conducted in female mice, which served as the primary cohort for formulation optimization.

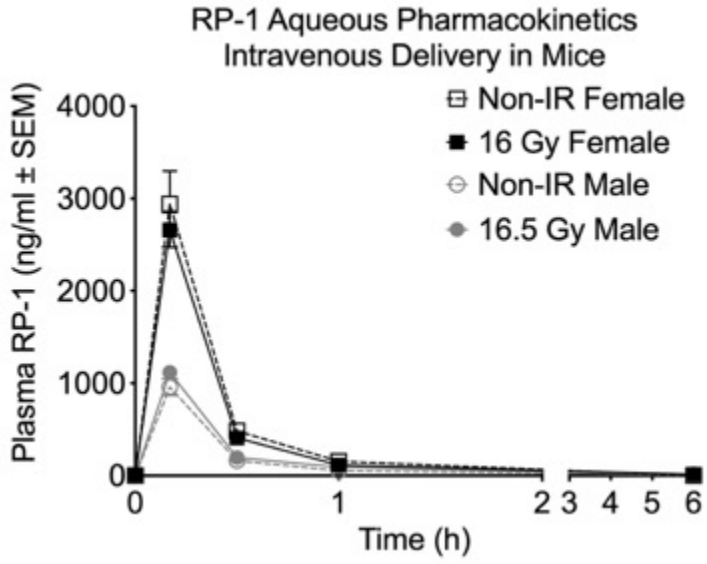

Figure 5. Sex but not irradiation affects the pharmacokinetic profile of RP-1 in mice. Non-irradiated and TBI (16-16.5 Gy) female and male mice, respectively, were dosed via tail vein injection with 3 mg/kg RP-1 in AQ formulation. Plasma samples were generated from 4-6 mice per time point, and RP-1 plasma concentration was quantified by LC-MS/MS. NCA was conducted using Phoenix WinNonlin 8.4.0 Figure adapted from the author's original publication (57).

Table 5. Pharmacokinetic Parameters of RP-1 in Irradiated vs Non-Irradiated Mice

	Female		Male	
Parameter	**Non-Irradiated**	**16.0 Gy**	**Non-Irradiated**	**16.5 Gy**
T_{max} (h)	0	0.70 ± 0.27	1.50 ± 0.58	1.50 ± 0.58
$t_{1/2}$ (h)	0.32 ± 0.13	1.15 ± 0.28	8.42 ± 1.16	8.42 ± 1.16
MRT (h)	0.27 ± 0.08	1.90 ± 0.13	8.58 ± 0.42	8.58 ± 0.42
AUC (ng/ml*h)	1507.8 ± 415.9	1069.8 ± 166.3	2573.8 ± 479.9	2573.8 ± 479.9
F (%)	100	71.0 ± 11.0	-	-
CL_T/F (ml/h/g)	2.05 ± 0.51	2.75 ± 0.41	1.02 ± 0.18	1.02 ± 0.18
CL_T (ml/h/g)	2.05 ± 0.51	1.95 ± 0.29	0.72 ± 0.12	0.72 ± 0.12

4.3 Extended-release RP-1 improves outcomes in GI-ARS

4.3.1 RP-1 ME mitigates GI-ARS

To determine whether pharmacokinetic optimization of RP-1 translated into improved mitigation efficacy, survival studies were conducted in the PBI-BM5 model of GI-ARS. Female C57BL/6J mice were exposed to 16.0–16.5 Gy and treated with 30 mg/kg RP-1 ME beginning 24 h post-irradiation. In the primary mitigation paradigm, a

second dose was administered at 72 h post-exposure. Kaplan-Meier survival analysis demonstrated a significant improvement in 21-day survival in mice treated with RP-1 ME compared to vehicle-treated controls. While vehicle-treated animals exhibited mortality consistent with the $LD_{70/21}$ model, RP-1 ME administration resulted in a marked increase in survival proportion over the observation period (**Figure 6B**). Statistical comparison using the Mantel-Cox log-rank test confirmed a significant difference between treatment groups. Alternative dosing paradigms were evaluated to assess timing sensitivity. Differences in end-point survival percentage were evident with administration of a single dose of RP-1 ME at 24 h post-irradiation; however, the overall Mantel-Cox log-rank test was not significantly difference (**Figure 6A**). Similarly, no survival benefit was noted when dosing was delayed to 48 h post-irradiation with a second dose at 96 h post-irradiation (**Figure 6C**).

When we extended the efficacy studies to male mice, RP-1 ME at a 30 mg/kg dose caused severe toxicity. A series of dose response efficacy studies were attempted in male mice to establish the dose that would provide a survival advantage while minimizing toxicity (**Figure 7**). While dual dosing with 5 mg/kg RP-1 ME at 24 h and 72 h post-irradiation provided slight end-point survival advantage to male mice, the overall log-rank analysis was not significant (**Figure 7B**). All other dosing paradigms attempted in male mice resulted in no survival advantage or marked toxicity. While we were unable to delay administration beyond 24 h post-irradiation or reduce the overall number of injections to one, we were able to optimize a RP-1 dosing regimen with considerably fewer injections using the ME formulation than previously necessary with the AQ formulation in the female GI-ARS model.

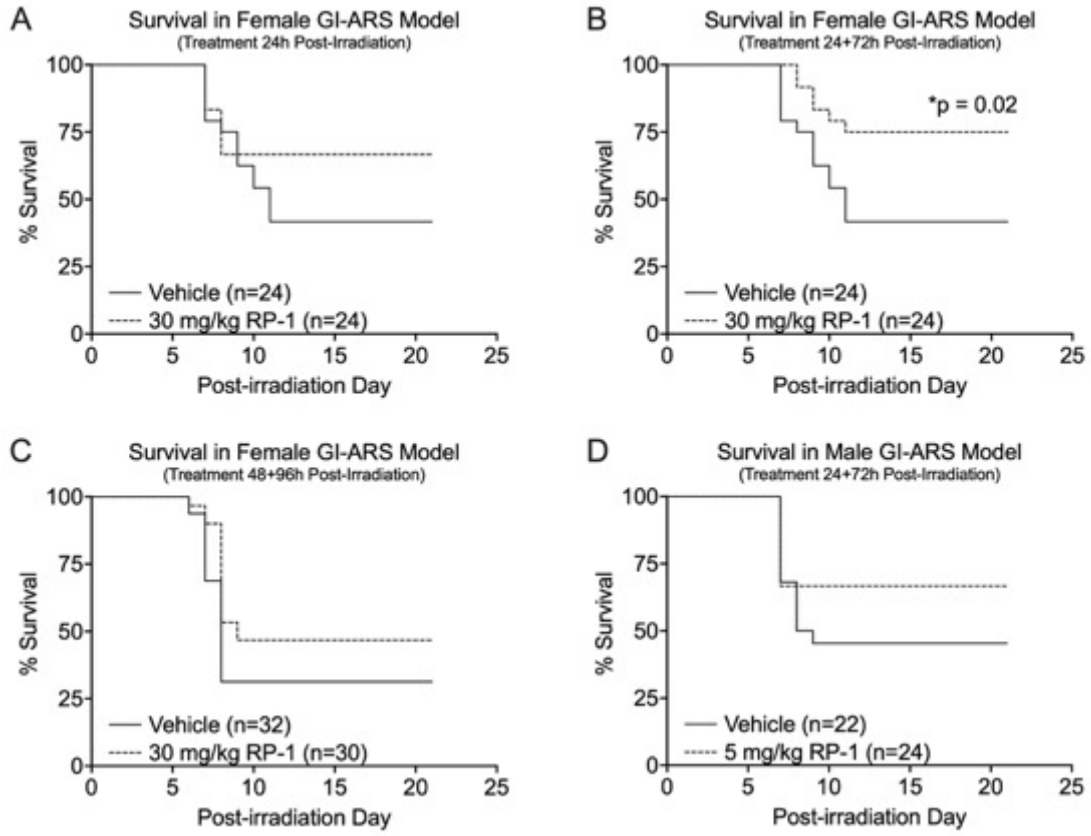

Figure 6. RP-1 ME mitigates GI-ARS. Female mice were exposed to 16 Gy PBI-BM5 and treated with vehicle or 30 mg/kg RP-1 ME in multiple treatment paradigms: (**A**) a single dose 24 h post-irradiation, (**B**) two doses 24 h and 72 h post-irradiation, or (**C**) two delayed doses at 48 h and 96 h post-irradiation. Kaplan-Meier plots were generated for percent survival, and Mantel-Cox log-rank analysis was conducted to compare vehicle vs RP-1 ME (n=22-32). Male mice were assessed in the same dual dosing regimen found effective in females using 5 mg/kg RP-1 ME due to observed toxicity (**D**). Figure adapted from the author's original publication (57).

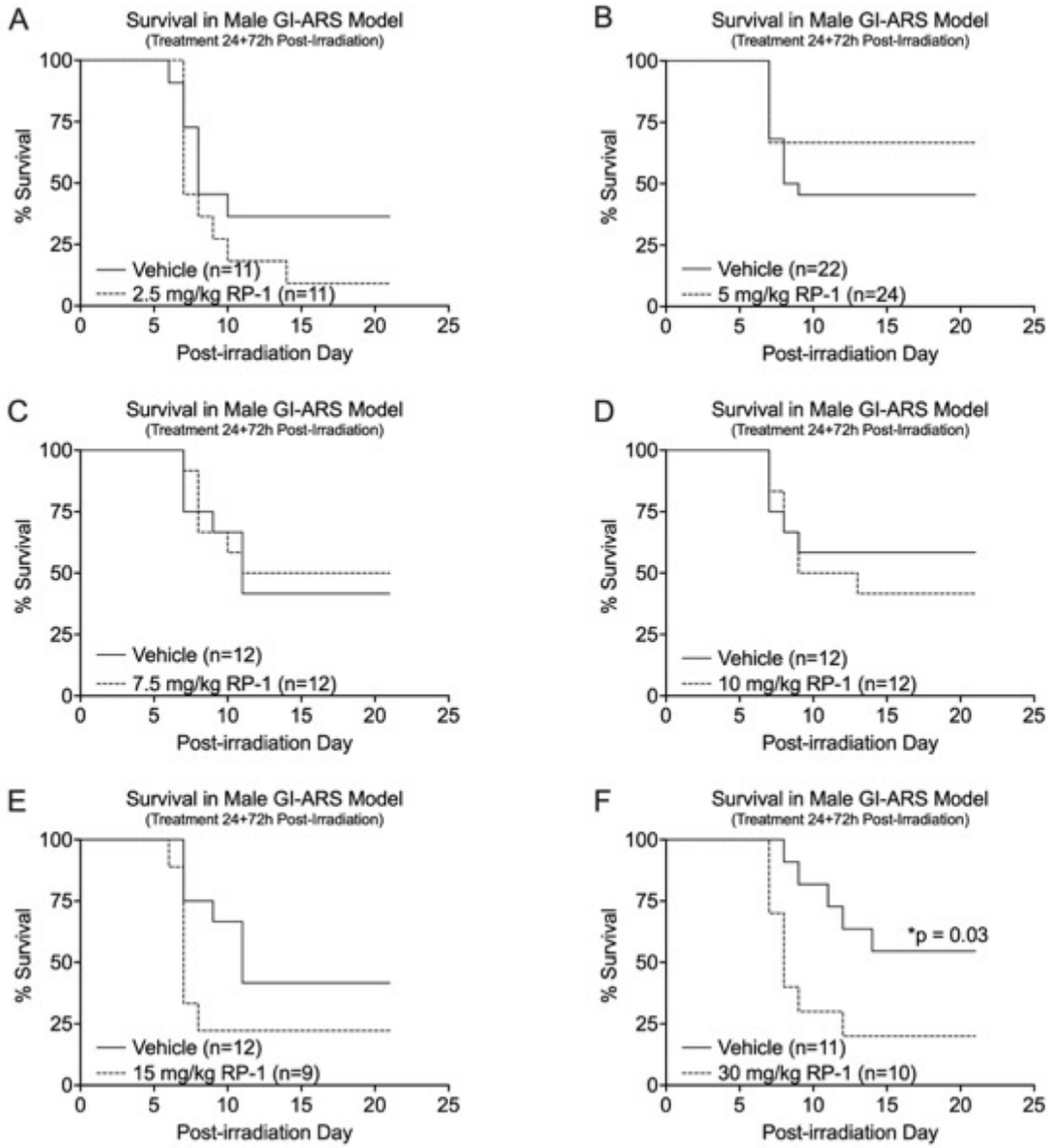

Figure 7. RP-1 ME exhibits toxicity in a male model of GI-ARS. Male mice were exposed to 16.5 Gy PBI-BM5 and treated with either vehicle or RP-1 ME at multiple concentrations ranging from 2.5-30 mg/kg administered 24 h and 72 h post-irradiation (A-F). Kaplan-Meier plots were generated for percent survival, and Mantel-Cox log-rank analysis was conducted to compare vehicle vs RP-1 ME (n=9-24). Figure adapted from the author's original publication (57).

4.3.2 RP-1 ME preserves intestinal crypt architecture and regeneration

We showed previously that AQ RP-1 increases the survival of cultured small intestine-derived enteroids by protecting Lgr5-positive ISC in intestinal crypts after radiation injury (56). To evaluate whether improved survival with RP-1 ME was associated with preservation of intestinal epithelial integrity, mice were irradiated in the PBI-BM5 model of GI-ARS and dosed with the effective 30 mg/kg RP-1 ME in the 24 h and 72 h paradigm. Histological assessment was then performed on post-irradiation day 5, corresponding to the anticipated crypt nadir in the GI-ARS model. Associated H&E-stained sections of jejunum from vehicle treated female mice demonstrated marked crypt depletion and architectural disruption. In contrast, RP-1 ME treated mice exhibited increased numbers of surviving crypts with preserved structural organization (**Figure 8A**). Quantitative analysis using the microcolony assay revealed a significant increase in the number of surviving crypts per circumference in RP-1 treated animals compared to vehicle controls. Immunohistochemical staining for Ki67 was performed on adjacent sections to assess proliferative activity within regenerating crypts. Vehicle treated mice exhibited limited Ki67-positive crypts. In contrast, RP-1 ME treated animals demonstrated an increased number of Ki67-positive crypts, indicating enhanced intestinal epithelial regenerative activity during the critical recovery phase (**Figure 8B**).

Together, these findings demonstrate that extended-release RP-1 administration beginning 24 h after irradiation significantly improves survival in a murine GI-ARS model and is associated with preservation of intestinal crypt architecture and proliferative capacity.

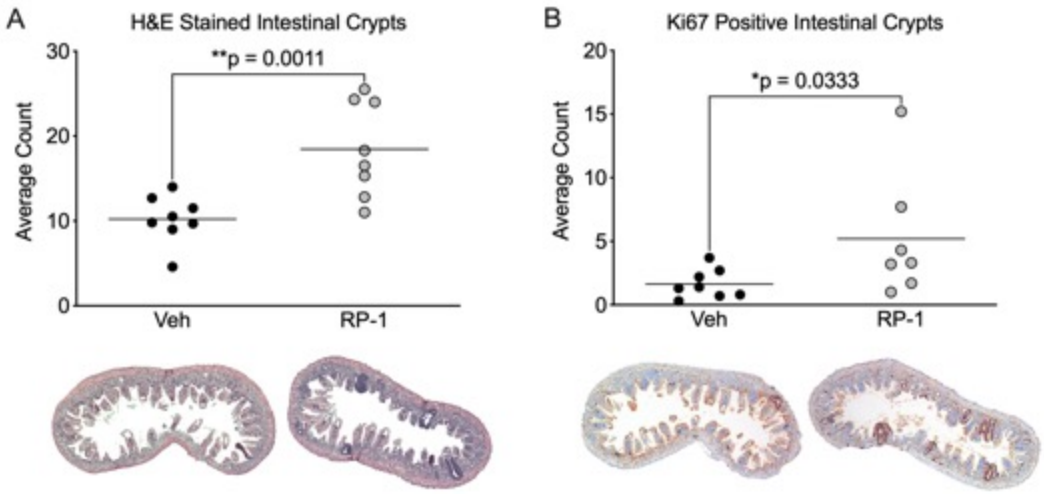

Figure 8. RP-1 ME preserves intestinal crypt architecture and regeneration. Female mice were irradiated in the PBI-BM5 model and treated with either vehicle or 30 mg/kg RP-1 ME 24 h and 72 h post-irradiation. Tissue sections were stained with H&E (**A**) for total crypt counting or used for immunohistochemical staining for Ki67 (**B**) for actively proliferating crypts. Intestinal crypts were counted from all three sections for each mouse using light microscopy by two independent investigators, and the average crypt count was compared for vehicle (n=8) vs RP-1 ME treated mice (n=7-8) using Student's unpaired t-test. Microscopy images are representative examples of multiple samples counted per treatment group. Figure adapted from the author's original publication (57).

4.4 LPAR activation promotes survival

4.4.1 RP-1 activates LPAR dependent prolonged pro-survival signaling

Previously, we showed that LPA, OTP, and DBIBB, sister compound to RP-1, activate ERK and Akt phosphorylation in LPAR2 expressing IEC-6 cells and MEF (36, 50, 52). To further characterize RP-1, phosphorylation time-course of ERK and Akt at two phosphorylation sites were assessed using a phospho-antibody cell-based ELISA technique over a 16 h time-course in EV and LPA2 MEF treated with RP-1 or vehicle and exposed to sham or 15 Gy irradiation. We noted robust ERK activation by LPA and RP-1 as early as 5 min in both sham and irradiated LPA2 MEF, with peak phosphorylation occurring at 1 h (**Figure 9A-B**). LPA induced greater ERK phosphorylation than RP-1 but declined after the 1 h peak, particularly in irradiated LPA2 MEF, whereas RP-1 sustained ERK phosphorylation in both sham and irradiated cells for up to 16 h.

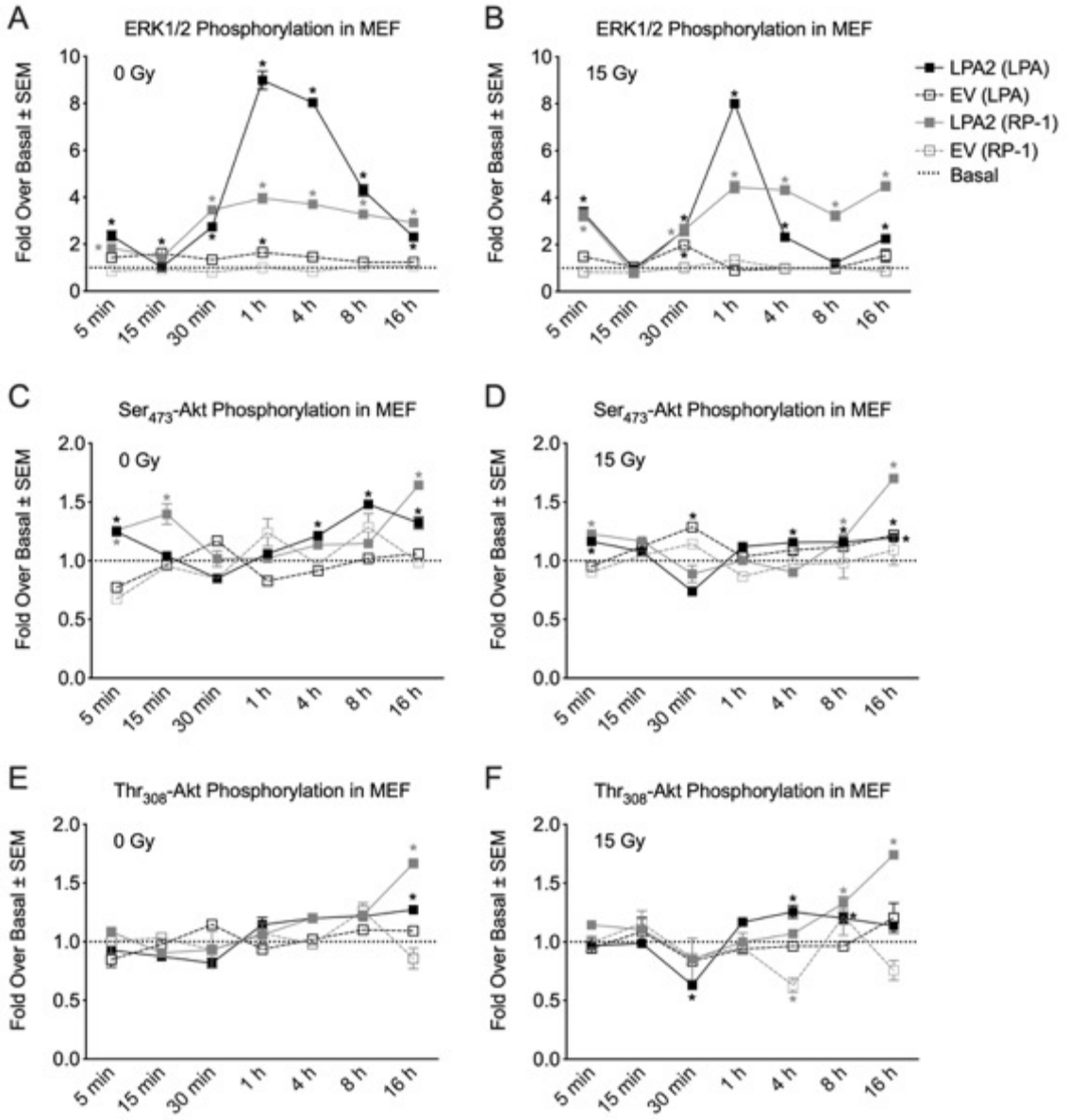

Figure 9. RP-1 activates LPAR dependent prolonged pro-survival signaling. Non-irradiated (**A**, **C**, **E**) and 15 Gy irradiated (**B**, **D**, **F**) EV and LPA2 MEF were treated with 10 μM LPA 18:1 or 10 μM RP-1. ERK (**A**-**B**) and Akt (**C**-**F**) phosphorylation were measured using PACE assay over a period of 16 h. Data were normalized to total ERK or total Akt within each treatment group, and two-factor ANOVA with Tukey's post hoc test was used to determine whether ERK or Akt activation differed significantly from basal levels (n=3 for each time point; *$p < 0.05$). Figure adapted from the author's original publication (57).

Next, we evaluated Akt phosphorylation at both Ser_{473} and Thr_{308} by LPA or RP-1. Ser_{473} Akt phosphorylation appeared biphasic in response to both LPA and RP-1 with detection within 5 min, diminished by 30 min, and subsequently increased out to 16 h in both sham and irradiated LPA2 MEF (**Figure 9C-D**). Comparatively, Thr_{308} Akt phosphorylation by LPA and RP-1 was markedly delayed to 4-8 h in irradiated LPA2 MEF and was only detectable at 16 h in sham LPA2 MEF (**Figure 9E-F**). Remarkably, for all three targets probed, RP-1 exhibited a greater level of phosphorylation at 16 h compared to LPA. Little to no ERK or Akt phosphorylation was noted in EV MEF, further supporting previous evidence that LPA or RP-1 induced long-duration activation of these pro-survival signaling kinases via LPAR2.

4.4.2 RP-1 prevents apoptosis

Our work has previously shown that LPA, OTP, and DBIBB protect LPAR2 expressing MEF and IEC-6 cells from apoptosis by reducing caspase 3/7 activation and increasing clonogenic survival post-irradiation (49, 50). To determine whether sustained kinase activation by RP-1 was associated with modulation of apoptotic signaling, caspase 3/7 activity was measured at 4 h, 8 h, and 16 h post-irradiation in EV and LPA2 MEF. At both 4 h and 8 h post-irradiation, caspase 3/7 activation was significantly elevated in both cell types (**Figure 10A-B**) and returned to baseline by 16 h post-irradiation (**Figure 10C**). RP-1 significantly reduced caspase 3/7 activation in LPA2 MEF at both 4 h and 8 h post-irradiation. This did not occur in EV MEF. Interestingly, the apoptotic response also resolved more quickly in LPA2 MEF vs EV MEF, as in both RP-1 treated and untreated cells, caspase activation at 8 h was markedly lower in LPAR2 expressing cells (**Figure 10B**).

Taken together, these data demonstrate that pharmacologic activation of LPAR signaling promotes prolonged pro-survival kinase activity and attenuates caspase-mediated apoptosis following irradiation *in vitro*.

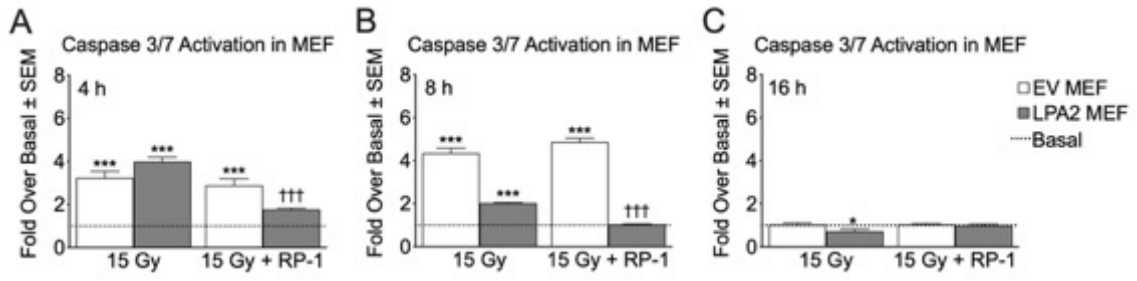

Figure 10. RP-1 prevents apoptosis. EV and LPA2 MEF were stimulated with 10 μM RP-1 for 15 min prior to 15 Gy irradiation. Caspase 3/7 activation was assessed at 4 h (**A**), 8 h (**B**), and 16 h (**C**) post-irradiation by Caspase-Glo 3/7 luminescence assay. Data were normalized to non-irradiated vehicle control within each cell type, and depicted as fold change over basal level. Two-factor ANOVA with Šídák's post hoc test was used to determine whether irradiation significantly increased caspase activation (n=3 for each time point; *$p < 0.05$, ***$p < 0.001$) and whether RP-1 significantly reduced the irradiation-induced effect ($^{\dagger\dagger\dagger}p < 0.001$). Figure adapted from the author's original publication (57).

4.5 IEX-1 deficiency exacerbates H-ARS and GI-ARS

Expression of IEX-1 is induced by radiation damage, and its functions in pro-survival and anti-apoptotic signaling control cell fate in the subsequent injury response (5, 44, 66-68). To determine whether IEX-1 contributes to survival following radiation exposure, WT and IEX-1 KO mice were evaluated in models of both H-ARS and GI-ARS. In the H-ARS model, mice were subjected to 9 Gy TBI, and survival was monitored for 30 days post-exposure (**Figure 11A**). In the GI-ARS model, WT and IEX-1 KO mice were subjected to 16 Gy PBI-BM5, and survival was monitored for 21 days following irradiation (**Figure 11B**). Kaplan-Meier analysis demonstrated approximately 30% reduced endpoint survival in IEX-1 KO mice compared to WT controls in both subsyndrome models. Statistical comparison using the Mantel-Cox log-rank test confirmed these significant differences between genotypes. Together, these findings demonstrate that IEX-1 deficiency increases radiosensitivity in both H- and GI-ARS.

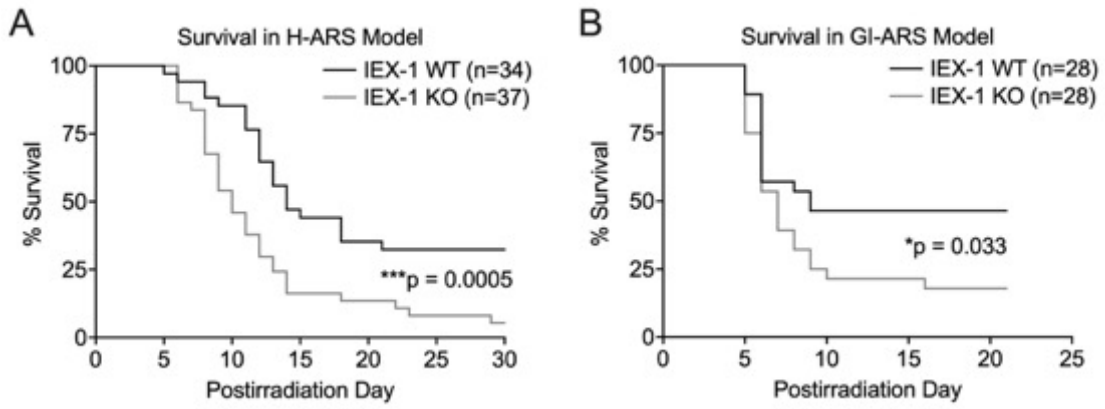

Figure 11. IEX-1 deficiency exacerbates H-ARS and GI-ARS. Female WT and IEX-1 KO mice were exposed to 9 Gy TBI (B) or 16 Gy PBI-BM5 (B). Kaplan-Meier plots were generated for percent survival, and Mantel-Cox log-rank analysis was conducted to compare WT vs IEX-1 KO (n=28-37). Figure adapted from the author's original manuscript (submitted under review).

4.6 IEX-1 regulates intestinal epithelial growth and ERK signaling dynamics

4.6.1 Loss of IEX-1 delays enteroid growth

To assess the impact of IEX-1 deficiency on intestinal epithelial regenerative capacity, three-dimensional small intestinal enteroid cultures were established from WT and IEX-1 KO mice. Enteroid growth and differentiation were monitored over a nine-day period under standard culture conditions. WT enteroids demonstrated progressive expansion and budding morphology consistent with active stem cell proliferation and differentiation. In contrast, IEX-1 KO enteroids exhibited delayed growth kinetics and reduced structural complexity (**Figure 12A**). Quantitative analysis revealed a significant lag in growth evidenced by decreased enteroid size (**Figure 12B**) and reduced budding (**Figure 12C**) in KO cultures compared to WT controls up to approximately day 7 in culture.

To determine whether IEX-1 deficiency resulted in detectable differences in intestinal architecture *in vivo*, H&E-stained sections of jejunal tissue from WT and KO mice were evaluated. No significant differences in total crypt number or gross crypt morphology were observed between genotypes under these conditions (**Figure 12D**). These findings indicate that while IEX-1 deficiency alters *ex vivo* intestinal epithelial growth dynamics, overt differences in crypt number were not detected *in vivo*.

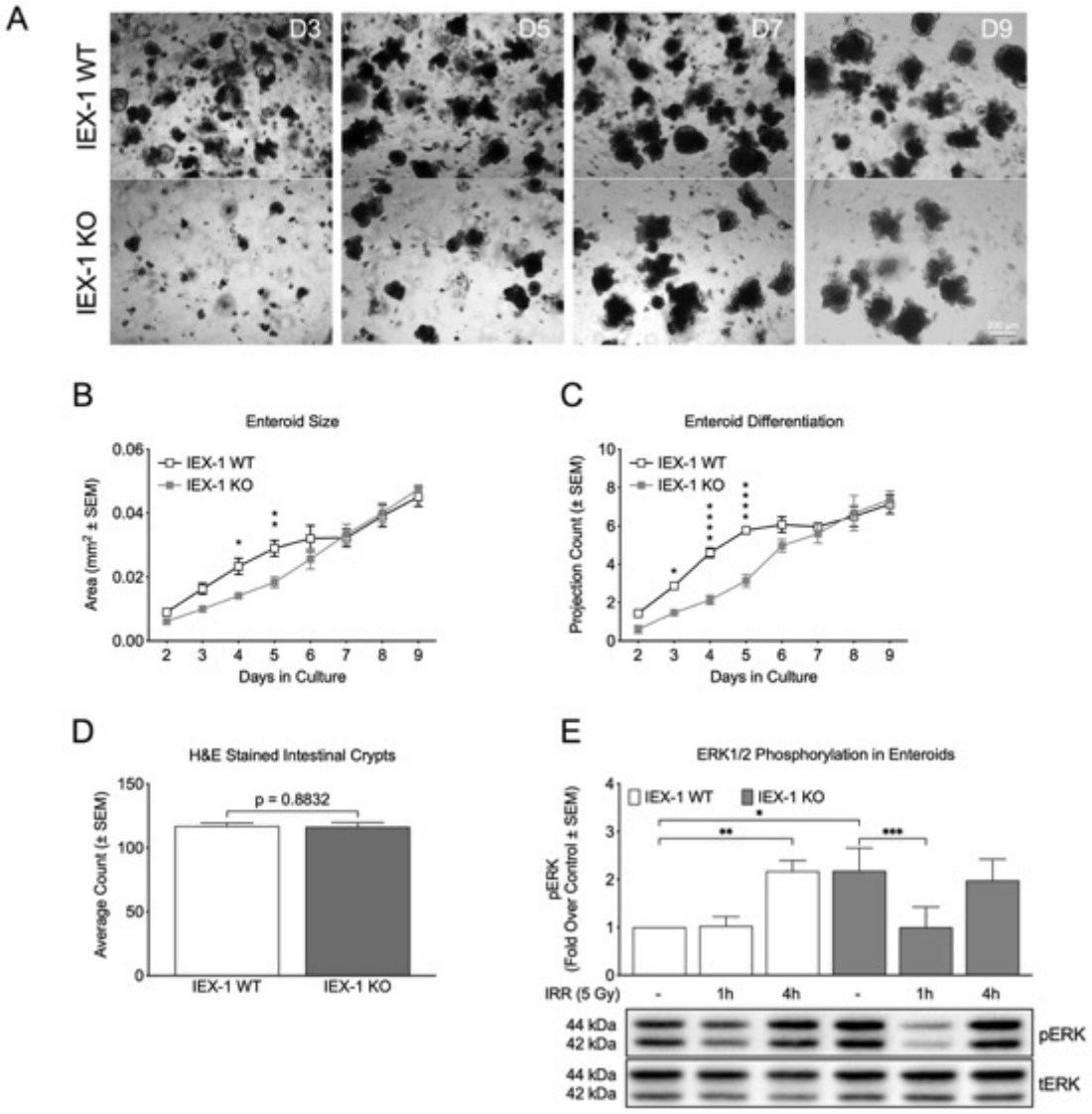

Figure 12. Loss of IEX-1 Delays Enteroid Growth and Alters ERK Signaling. Enteroids from female WT or IEX-1 KO mice were monitored daily over a 9-day period (**A**). Growth and differentiation were quantified as mean area (**B**) and number of budding structures (**C**). Data were analyzed by two-way ANOVA with Tukey's post hoc test (n=3 independent isolations; *p < 0.05, **p < 0.01, ****p < 0.0001). Jejunal crypt numbers were quantified from H&E-stained sections (**D**) and compared by unpaired t-test (n=5 per genotype). WT and IEX-1 KO enteroids were exposed to sham or 5 Gy irradiation and harvested at 1 h or 4 h post-irradiation. Phosphorylated ERK1/2 levels were normalized to total ERK1/2 and represented relative to non-irradiated WT controls (**E**). Statistical analysis was performed by two-way ANOVA with Tukey's post hoc test (n=3; *p < 0.05, **p < 0.01, ***p < 0.001). Immunoblot is representative of 3 independent experiments. Figure adapted from the author's original manuscript (submitted under review).

4.6.2 Loss of IEX-1 alters ERK signaling

It has been established that IEX-1 participates in ERK pathway regulation (38, 39, 41, 66). To evaluate whether altered growth characteristics were associated with differences in pro-survival signaling, ERK phosphorylation was examined by immunoblot in WT and IEX-1 KO enteroids following irradiation. In WT enteroids, irradiation had little effect at 1 h but resulted in a ~2-fold increase in ERK phosphorylation at 4 h post-exposure (**Figure 12E**). In contrast, IEX-1 KO enteroids exhibited altered ERK signaling kinetics characterized by elevated basal phosphorylation levels (~2-fold higher than WT) with reduced ERK phosphorylation at 1 h post-irradiation. Densitometric analysis of immunoblots demonstrated significant differences in phospho-ERK levels between genotypes at defined time points. These findings indicate that IEX-1 deficiency disrupts the activation of ERK in response to radiation.

4.6.3 LPAR stimulation induces IEX-1 expression

To evaluate the tissue distribution of IEX-1 expression in compartments relevant to radiation injury, RT-qPCR was performed on whole blood, intestinal mucosa, and small intestinal enteroid cultures. Baseline analysis demonstrated that IEX-1 transcript levels were ~15-fold higher in intestinal mucosal tissue relative to peripheral blood (**Figure 13A**). Enteroid cultures exhibited IEX-1 expression levels comparable to those observed in intact intestinal mucosa, consistent with epithelial compartmental enrichment. To assess receptor context, expression profiling of LPAR subtypes revealed LPAR2, LPAR5, and LPAR6 expression across all tissues, predominant LPAR1 and LPAR3 expression in intestinal mucosa, and complete absence of LPAR4 across all tissues (**Figure 13B**).

We have shown previously that LPAR2 expression is upregulated after radiation exposure (36), and stimulation of LPAR2 protects cells from radiation-induced apoptosis (56, 57, 69). To determine whether IEX-1 expression is responsive to LPAR stimulation, gene expression analysis was performed following *in vivo* and *ex vivo* LPAR activation by LPA and/or OTP. In whole blood, irradiation induced a ~4-fold increase in IEX-1 expression, and LPAR stimulation by OTP resulted in an additional ~10-fold increase relative to untreated controls 3 h post-irradiation (**Figure 14A**). In

intestinal mucosal samples, IEX-1 expression was not induced by irradiation, but LPAR stimulation by OTP resulted in ~5-fold increase in IEX-1 expression (**Figure 14B**). Similarly, in enteroid cultures expression of IEX-1 was not induced by irradiation alone, but LPAR stimulation by LPA and OTP resulted in upregulation of IEX-1 expression compared to baseline conditions at both 1 h and 3 h post-irradiation (**Figure 14C**). These findings demonstrate that IEX-1 expression is inducible in blood and intestinal epithelial cells following LPAR activation.

Collectively, these data establish that IEX-1 is expressed in radiation-relevant tissues, that LPAR2 is present in intestinal epithelial tissue, and that IEX-1 expression is responsive to LPAR stimulation.

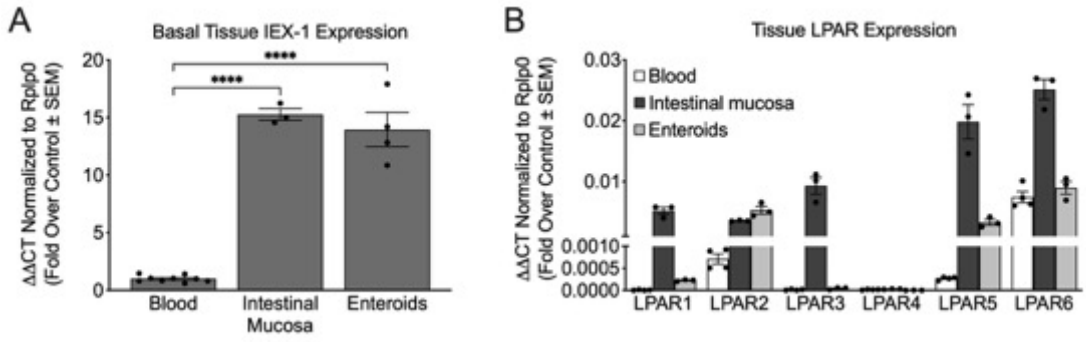

Figure 13. Tissue IEX-1 and LPAR Expression. IEX-1 (**A**) and LPAR1-6 (**B**) mRNA expression were assessed in whole blood, intestinal mucosa, and enteroids from female WT mice. Expression was quantified by RT-qPCR and normalized to *Rplp0*. Data represent mean fold change ± SEM. Statistical significance was determined by one-way ANOVA with Tukey's post hoc test (n=3-11; ****$p < 0.0001$). Figure adapted from the author's original manuscript (submitted under review).

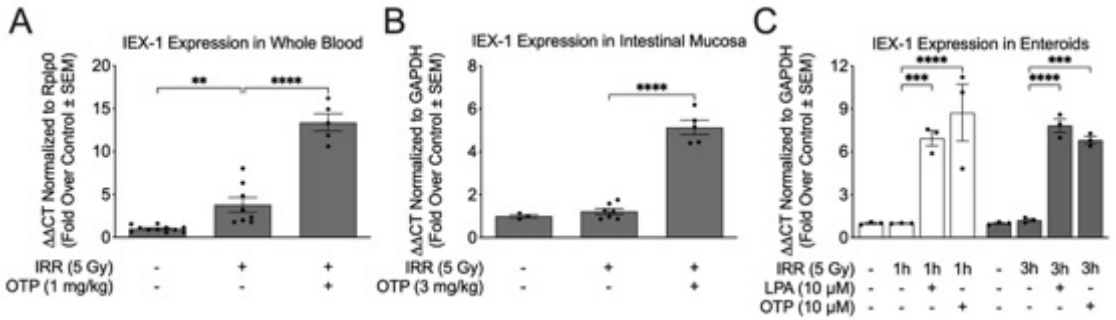

Figure 14. LPAR stimulation induces IEX-1 expression. Female WT mice were pre-treated with OTP for 30 min prior to sham, 9 Gy TBI (**A**), or 16 Gy PBI-BM5 (**B**), followed by collection of whole blood or intestinal mucosa 3 h post-irradiation. WT enteroids were pre-treated with LPA or OTP for 2 h, exposed to sham or 5 Gy irradiation, and harvested 1 h or 3 h post-irradiation (**C**). IEX-1 mRNA expression was quantified by RT-qPCR and normalized to *Rplp0* or *Gapdh*. Data represent mean fold change ± SEM. Statistical significance was determined by one-way ANOVA with Tukey's post hoc test (n=3-11; **p < 0.01, ***p < 0.001, ****p < 0.0001). Figure adapted from the author's original manuscript (submitted under review).

5. Discussion

ARS remains a major medical challenge following high-dose γ-radiation exposure. Injury to the hematopoietic and gastrointestinal systems represents the primary determinants of morbidity and mortality, yet effective countermeasures for GI-ARS remain limited. While several agents have been approved for treatment of hematopoietic injury, therapeutic strategies that mitigate intestinal radiation damage and support gastrointestinal epithelial regeneration are still needed.

The work presented in this thesis aimed to investigate signaling pathways that regulate cellular survival following radiation exposure and to evaluate pharmacologic strategies capable of enhancing tissue resilience. Using complementary pharmacologic and genetic approaches, these studies examined the roles of LPAR signaling in the context of the immediate early response gene IEX-1 in the response to radiation injury. The results demonstrate that pharmacologic activation of LPAR2 improves survival and preserves intestinal architecture in a murine model of GI-ARS, while genetic loss of IEX-1 increases radiosensitivity in both H- and GI-ARS mouse models. The following sections integrate these findings within the broader context of radiation biology and translational countermeasure development.

5.1 LPAR signaling as a strategic target for gastrointestinal radiomitigation

The gastrointestinal epithelium is among the most radiosensitive tissues in the body, and severe injury to the intestinal crypt niche is a defining feature of GI-ARS (16, 21). Following high-dose radiation exposure, loss of rapidly proliferating crypt stem cells leads to collapse of the crypt–villus architecture, deprivation of nutrients, impaired intestinal epithelial barrier function, and translocation of luminal bacteria and endotoxins into the systemic circulation (9, 10, 76). These events lead to sepsis, multi-organ failure, and mortality following high-dose radiation exposure (53, 77). Despite the critical role of intestinal injury in ARS pathogenesis, currently approved radiation countermeasures primarily target hematopoietic recovery, highlighting the need for strategies that directly address gastrointestinal injury (13, 31).

The findings presented in this thesis support existing literature on LPAR signaling as a promising therapeutic target for the mitigation of GI-ARS. Pharmacologic

activation of LPAR2 using the selective agonist RP-1 significantly improved survival in a murine PBI-BM5 model of GI-ARS when treatment was initiated 24 h after radiation exposure. Importantly, this survival benefit was accompanied by preservation of intestinal crypt architecture and increased numbers of regenerating crypts during the critical phase of epithelial recovery. These observations substantiate our previous findings that LPAR2 activation enhances intestinal epithelial resilience following radiation injury and supports regeneration of the crypt compartment during the period in which stem cell loss would otherwise compromise intestinal recovery (36, 52).

Mechanistically, LPAR stimulation was associated with sustained activation of pro-survival signaling pathways following irradiation. *In vitro* experiments demonstrated prolonged phosphorylation of ERK and Akt in MEF treated with either LPA or RP-1. This sustained kinase activation corresponded with reduced caspase-3/7 activity, indicating attenuation of apoptosis following radiation exposure. These observations are consistent with prior studies that showed pharmacologic inhibition of ERK and Akt signaling pathways abrogates LPA-mediated anti-apoptotic effects (43). As such, LPAR signaling engages downstream ERK and Akt pathways to regulate cellular survival and stress responses (43, 50, 51), including resistance to radiation-induced apoptosis and recovery of irradiated intestinal epithelial cells (32, 50, 51).

In addition to demonstrating biological efficacy, the present work highlights the importance of pharmacokinetic optimization in the development of practical radiation countermeasures. Earlier formulations of RP-1 required multiple injections over several days to maintain effective systemic exposure. Development of a multilayered W/O/W ME formulation substantially extended the plasma residence time of RP-1, enabling effective mitigation with a simplified two-dose regimen administered at 24 h and 72 h post-irradiation. From a translational perspective, such a dosing schedule is far more compatible with deployment in mass-casualty scenarios, where rapid distribution and limited medical resources may constrain treatment options.

The extended-release formulation also illustrates a broader principle in countermeasure development: sustained receptor engagement may be necessary to maintain protective signaling during the evolving phases of radiation injury. The improved pharmacokinetic profile achieved with the ME formulation may further extend prolonged activation of ERK and Akt observed following RP-1 treatment,

thereby supporting cell survival during the period of maximal damage.

An additional consideration emerging from this work is the potential influence of biological variables such as sex on treatment response. While significant survival benefit was observed in female mice treated with RP-1 ME, higher-dose administration in male mice was associated with toxicity, necessitating dose adjustment and resulting in a more modest survival effect under the conditions tested. Although the mechanistic basis for this difference remains unclear—and it is limited to mice as toxicity was not observed in male NHP—the observation highlights the importance of evaluating sex-specific pharmacologic responses during the development of radiation countermeasures.

Taken together, these findings demonstrate that pharmacologic activation of LPAR2 promotes intestinal epithelial survival following radiation exposure and that optimization of drug delivery can significantly enhance the translational feasibility of this approach. The ability of LPAR signaling to modulate pro-survival kinase pathways and support intestinal regeneration solidifies this pathway as a promising target for the development of medical countermeasures aimed at mitigating gastrointestinal radiation injury.

5.2 IEX-1 as a determinant of tissue radiosensitivity

IEX-1 was originally identified as a radiation-inducible immediate early gene whose expression is rapidly upregulated in response to cellular stress (37, 64, 65). IEX-1 functions as a stress-responsive adaptor protein capable of integrating multiple signaling inputs that regulate cell survival and apoptosis (65), and previous studies have demonstrated that IEX-1 expression can be induced by diverse stimuli including ionizing radiation, inflammatory cytokines, and oxidative stress through pathways involving p53, NF-κB, and ERK signaling (37, 65, 66, 78). As such, understanding the role of IEX-1 in early adaptive responses to irradiation is crucial in developing medical countermeasures aimed at mitigating ARS.

In addition to pharmacologic modulation of survival signaling through LPAR activation, the studies presented in this thesis identify IEX-1 as an important determinant of radiation sensitivity *in vivo*. Genetic deletion of IEX-1 resulted in significantly reduced survival in models of both H- and GI-ARS. The survival phenotype observed in IEX-1 KO mice following irradiation indicates that loss of IEX-1

increases susceptibility to radiation-induced injury in multiple tissue compartments. Previous work has demonstrated that IEX-1 contributes to hematopoietic recovery following radiation exposure by regulating oxidative stress in HSPC (79). In that context, IEX-1 deficiency leads to increased ROS accumulation and impaired recovery of erythroid and myeloid lineages following irradiation. The reduced survival observed in the present study following TBI is consistent with these earlier findings and further supports a role for IEX-1 in maintaining hematopoietic resilience during radiation injury.

The present work extends these observations by demonstrating that IEX-1 deficiency also increases susceptibility to gastrointestinal radiation injury. Although no significant differences in intestinal crypt number were observed between WT and IEX-1 KO mice, enteroid cultures derived from IEX-1 KO mice exhibited delayed growth and reduced structural complexity relative to WT controls. This *ex vivo* phenotype suggests that IEX-1 may contribute to intestinal epithelial regenerative capacity under conditions of stress when steady-state intestinal architecture appears largely preserved *in vivo*.

At the signaling level, IEX-1-deficiency was associated with altered ERK activation kinetics following irradiation. Specifically, IEX-1 KO enteroids exhibited elevated basal ERK phosphorylation but reduced early ERK activation following radiation exposure compared to WT cultures. These findings are consistent with prior studies indicating that IEX-1 participates in feedback regulation of ERK signaling (66). IEX-1 has been shown to interact with components of the PP2A phosphatase complex, which modulates ERK phosphorylation dynamics and contributes to regulation of cell survival pathways (38, 39, 66). Disruption of this regulatory network may therefore alter the temporal dynamics of ERK activation during cellular stress responses.

In addition to its role in ERK regulation, IEX-1 has been implicated in the control of mitochondrial ROS production through interactions with IF1 (44). By promoting degradation of IF1, IEX-1 enhances ATP synthase activity and limits excessive mitochondrial ROS accumulation, thereby reducing activation of downstream apoptotic pathways (44). This mechanism provides a potential explanation for the increased radiosensitivity observed in IEX-1 KO mice, as radiation-induced oxidative stress is a major contributor to cellular damage following ionizing radiation exposure (80).

Importantly, gene expression analyses performed in the present study demonstrated that IEX-1 is enriched in intestinal mucosal tissue relative to peripheral blood and is inducible following irradiation and LPAR stimulation in both blood and intestinal epithelial cells. These findings suggest that IEX-1 participates in stress-responsive signaling networks activated during radiation injury and may contribute to intestinal epithelial survival pathways downstream of LPAR signaling.

Taken together, the genetic findings presented in this thesis establish IEX-1 as a regulator of radiation response in both hematopoietic and gastrointestinal tissues. While additional work will be required to define the precise molecular interactions linking IEX-1 to specific survival pathways, the combined survival, enteroid growth, and signaling data indicate that IEX-1 plays an important role in modulating cellular responses to radiation-induced stress.

5.3 Integration of LPAR signaling and IEX-1 regulation in radiation response

The pharmacologic and genetic findings presented in this thesis collectively suggest that LPAR signaling and IEX-1 may participate in a shared regulatory network that influences cellular responses to radiation injury. Although the precise molecular relationship between these pathways is not fully defined, several observations from the present work indicate that they may converge on common pro-survival signaling mechanisms.

Pharmacologic activation of LPAR2 using RP-1 resulted in sustained phosphorylation of ERK and Akt following irradiation and was associated with reduced caspase-mediated apoptosis *in vitro*. Activation of these pathways has been shown to attenuate radiation-induced apoptosis and promote recovery of damaged intestinal epithelial tissues. In parallel with these pharmacologic observations, genetic deletion of IEX-1 produced alterations in ERK signaling kinetics following irradiation. This altered temporal pattern of ERK signaling suggests that IEX-1 may function as a regulatory component that modulates the magnitude and duration of ERK pathway activation during cellular stress responses. In addition to these signaling effects, we demonstrated that IEX-1 expression is further induced following stimulation of LPAR signaling. This inducible expression pattern suggests that IEX-1 may be part of a broader transcriptional response triggered by LPAR-mediated signaling during cellular stress.

Taken together, these findings are consistent with a model in which LPAR activation promotes pro-survival signaling following radiation exposure and induces expression of stress-responsive genes such as IEX-1 that may contribute to regulation of downstream signaling dynamics. In this framework, IEX-1 may function as a modulatory component that helps shape ERK signaling responses during radiation-induced stress, thereby influencing cell survival and tissue recovery.

Importantly, the present studies do not directly establish a causal signaling axis linking LPAR activation to ERK regulation through IEX-1. The pharmacologic and genetic datasets were generated independently and therefore cannot determine whether IEX-1 is required for the pro-survival signaling effects observed following LPAR stimulation. Additional experiments, such as assessing LPAR-mediated signaling responses in IEX-1-deficient cells and tissues, would be required to determine whether IEX-1 functions as a necessary mediator of this pathway. Nevertheless, the convergence of pharmacologic and genetic observations suggests that LPAR-mediated signaling and IEX-1 regulation may represent complementary components of cellular defense mechanisms activated following radiation exposure. Understanding how these pathways interact may provide further insight into the molecular determinants of tissue radiosensitivity and may help identify new opportunities for therapeutic intervention.

5.4 Translational implications for radiation countermeasure development

The development of medical countermeasures capable of mitigating radiation injury remains a priority for both public health preparedness and clinical radiation medicine. Large-scale radiological or nuclear incidents would likely produce varied patterns of injury involving both hematopoietic and gastrointestinal organ systems. While several agents have received regulatory approval for treatment of the hematopoietic subsyndrome of ARS, including granulocyte colony-stimulating factor-based therapies such as filgrastim, pegfilgrastim, and sargramostim, there are currently no approved therapeutics specifically targeting gastrointestinal radiation injury (13, 81). As a result, GI-ARS continues to represent a critical unmet need in the field of radiation countermeasure development.

The findings presented in this thesis highlight LPAR signaling as a potential target for therapeutic intervention in GI-ARS. Pharmacologic activation of LPAR2

using the selective agonist RP-1 improved survival and preserved intestinal crypt architecture in a murine model of GI-ARS when treatment was initiated 24 h following irradiation. Importantly, this post-exposure treatment window is consistent with the operational constraints that would be expected following a mass-casualty radiological incident, where immediate medical intervention may not be feasible for all affected individuals.

Another key translational consideration addressed in the present work is the importance of drug formulation and pharmacokinetic optimization. Many candidate radiation countermeasures demonstrate biological activity in experimental models but face practical limitations related to dosing frequency or delivery logistics. Development of the multilayered W/O/W ME formulation of RP-1 significantly extended systemic drug exposure and enabled effective mitigation with a simplified two-dose regimen administered at 24 h and 72 h post-irradiation. From an operational standpoint, such a dosing schedule is substantially more feasible for deployment in emergency response scenarios than regimens requiring repeated daily administration.

The observation that LPAR activation promotes sustained pro-survival signaling pathways further supports the potential translational value of this therapeutic strategy. Radiation injury evolves over several days as cellular damage, inflammatory responses, and regenerative processes unfold. Therapeutic approaches that maintain protective signaling during this dynamic injury phase may therefore provide greater benefit than interventions that act only during the immediate post-irradiation period.

In addition to pharmacologic considerations, the genetic findings presented in this work underscore the importance of further exploring endogenous stress-response pathways in determining tissue radiosensitivity. Identification of IEX-1 as a regulator of survival in both H- and GI-ARS models highlights the broader concept that modulation of stress-responsive signaling networks may represent a viable approach for improving tissue resilience following radiation exposure. Understanding the molecular pathways that influence radiosensitivity may therefore facilitate identification of additional therapeutic targets for countermeasure development.

These findings contribute to the growing body of research aimed at developing effective treatments for radiation-induced normal tissue injury. Continued investigation of LPAR-mediated signaling pathways and their downstream regulatory networks may

provide new opportunities for the development of radiomitigators capable of addressing the currently unmet need for therapies targeting gastrointestinal radiation injury.

5.5 Limitations and future directions

The studies presented in this work provide new insight into signaling pathways that influence radiation response; however, several limitations should be considered when interpreting these findings and in guiding future investigation.

First, while pharmacologic activation of LPAR signaling confers significant mitigation of gastrointestinal radiation injury, the precise molecular mechanisms underlying these highly complex and interlinked protective effects remain incompletely defined. The present work showed that LPAR stimulation promotes sustained ERK and Akt activation and reduces caspase-mediated apoptosis following irradiation. Previous studies have shown that LPAR2 signaling can engage adaptor proteins such as TRIP6 and NHERF2 and activate downstream ERK and Akt pathways (46) and regulates DNA repair by enhancing γH2AX histone phosphorylation (36). Further investigation will be required to determine how these signaling complexes and repair mechanisms contribute to intestinal epithelial survival and regeneration during radiation injury.

Second, the genetic studies identifying IEX-1 as a determinant of radiosensitivity were performed using a global KO model. Because IEX-1 is expressed in multiple tissues, the relative contribution of individual cellular compartments to the observed survival phenotype cannot be determined from the present experiments. Conditional KO models targeting intestinal epithelial cells or HSPC would help clarify the tissue-specific functions of IEX-1 in radiation response.

Another limitation relates to the mechanistic relationship between LPAR signaling and IEX-1 regulation. The present studies demonstrated that IEX-1 expression is inducible following LPAR stimulation and that IEX-1 deficiency alters ERK signaling kinetics following irradiation. However, the experiments presented here do not directly establish whether IEX-1 is required for the protective signaling effects elicited by LPAR activation. Future studies evaluating LPAR-mediated signaling responses in IEX-1-deficient systems will help determine whether IEX-1 functions as a downstream mediator of LPAR signaling or whether these pathways operate independently within a broader radiation-responsive network.

The present work also identified alterations in ERK signaling dynamics in IEX-1 KO enteroids, suggesting that IEX-1 may influence the temporal regulation of this pathway during cellular stress responses. Previous studies have proposed that IEX-1 interacts with components of the PP2A phosphatase complex and may regulate mitochondrial oxidative stress through interactions with IF1 (38, 39, 44). Additional molecular studies will be required to determine how these mechanisms contribute to radiation response in intestinal epithelial tissues.

Finally, while the pharmacokinetic and efficacy studies support the translational potential of RP-1 as a radiation mitigator, additional work will be necessary to evaluate the broader applicability of this therapeutic strategy. Future studies examining dose optimization, treatment regimen, and efficacy across multiple biological variables—including sex and different radiation injury models—will help define the therapeutic window and safety profile of LPAR-targeted interventions. Evaluation in additional preclinical models will also be important for advancing this approach toward clinical development as a medical countermeasure.

Despite these limitations, the combined findings presented here provide a framework for further investigation into signaling pathways that regulate tissue radiosensitivity and support the continued development of therapeutic strategies targeting radiation-induced gastrointestinal injury.

6. Conclusions

This work investigated signaling pathways that regulate cellular responses to ionizing radiation and explored strategies for mitigating radiation-induced injury. Using complementary pharmacologic and genetic approaches, the studies presented here examined the role of LPAR signaling and IEX-1 in determining survival outcomes following radiation exposure. The principal conclusions are as follows:

- **Activation of LPAR signaling mitigates GI-ARS.** Treatment with the selective LPAR2 agonist RP-1 improved survival and preserved intestinal crypt architecture in a murine GI-ARS model when administered beginning 24 h post-irradiation.
- **Pharmacokinetic optimization improves the translational feasibility of RP-1.** A multilayered W/O/W ME formulation extended the plasma residence time of RP-1 in both mice and NHP and enabled effective radiation mitigation with a simplified two-dose regimen in a murine GI-ARS model.
- **LPAR activation promotes sustained pro-survival signaling following irradiation.** Stimulation with LPA or RP-1 resulted in prolonged ERK and Akt phosphorylation and reduced caspase-mediated apoptosis *in vitro* in MEF.
- **IEX-1 is a determinant of tissue radiosensitivity.** IEX-1 KO mice exhibited reduced survival in models of both H- and GI-ARS, indicating that IEX-1 contributes to radiation injury response in multiple tissue compartments.
- **IEX-1 influences intestinal epithelial growth dynamics and ERK signaling responses.** Enteroids derived from IEX-1 KO mice displayed delayed growth and altered ERK phosphorylation kinetics following irradiation, and IEX-1 expression was inducible following LPAR stimulation, implying that IEX-1 participates in stress-responsive signaling networks that regulate cellular responses to radiation-induced damage.

Collectively, these findings highlight the importance of survival signaling pathways in determining tissue responses to radiation exposure. The results support continued investigation of LPAR-targeted therapeutics and identify IEX-1 as a regulator of radiosensitivity that may contribute to future strategies for mitigating radiation-induced injury.

7. Summary

The primary drivers of ARS-related mortality are systemic injuries to the hematopoietic and gastrointestinal systems. Give the lack of robust countermeasures for GI-ARS, this research focused on the regulatory signaling pathways triggered by radiation injury. Specifically, we investigated novel pharmacologic approaches to mitigate cellular injury and improve overall outcomes.

The first component of this research examined pharmacologic activation of LPAR signaling as a strategy for mitigating gastrointestinal radiation injury. In a murine model of GI-ARS, treatment with the selective LPAR2 agonist RP-1 significantly improved survival when administered beginning 24 h after irradiation. RP-1 treatment also preserved intestinal crypt architecture and increased the number of regenerating crypts during the critical phase of intestinal epithelial recovery. *In vitro* experiments demonstrated that LPAR activation promotes sustained phosphorylation of ERK and Akt and reduces caspase-mediated apoptosis following irradiation, indicating that LPAR signaling enhances pro-survival responses during radiation-induced injury. Development of an extended-release W/O/W ME formulation improved the pharmacokinetic profile of RP-1 and enabled effective mitigation using a simplified dosing regimen.

The second component of this thesis investigated the role of IEX-1 in regulating tissue radiosensitivity. Genetic deletion of IEX-1 resulted in significantly reduced survival in murine models of both H- and GI-ARS. In addition, small intestinal enteroids derived from IEX-1 KO mice exhibited delayed growth and altered ERK signaling kinetics following irradiation. Gene expression analyses further demonstrated that IEX-1 is enriched in intestinal mucosa and inducible following stimulation of LPAR signaling.

Together, these findings demonstrate that survival signaling pathways play an important role in determining tissue responses to radiation exposure. The results identify LPAR signaling as a promising therapeutic target for mitigation of gastrointestinal radiation injury and establish IEX-1 as a regulator of tissue radiosensitivity, providing a basis for further investigation into mechanisms governing radiation response and the development of improved radiation countermeasures.

8. References

1. Waselenko JK, MacVittie TJ, Blakely WF, Pesik N, Wiley AL, Dickerson WE, Tsu H, Confer DL, Coleman CN, Seed T, Lowry P, Armitage JO, Dainiak N, Strategic National Stockpile Radiation Working G. Medical management of the acute radiation syndrome: recommendations of the Strategic National Stockpile Radiation Working Group. Ann Intern Med. 2004 Jun 15;140(12):1037-51. PubMed PMID: 15197022.

2. Mettler FA, Jr., Voelz GL. Major radiation exposure--what to expect and how to respond. N Engl J Med. 2002 May 16;346(20):1554-61. PubMed PMID: 12015396.

3. Dainiak N. Hematologic consequences of exposure to ionizing radiation. Exp Hematol. 2002 Jun;30(6):513-28. PubMed PMID: 12063018.

4. Hall EJ, Giaccia AJ. Radiobiology for the radiologist. Eighth edition. ed. Philadelphia: Wolters Kluwer; 2019. vii, 597 pages p.

5. Pawlikowska P, Leray I, de Laval B, Guihard S, Kumar R, Rosselli F, Porteu F. ATM-dependent expression of IEX-1 controls nuclear accumulation of Mcl-1 and the DNA damage response. Cell Death Differ. 2010 Nov;17(11):1739-50. PubMed PMID: 20467439. PMCID: PMC3923326. Epub 20100514.

6. Heslet L, Bay C, Nepper-Christensen S. Acute radiation syndrome (ARS) - treatment of the reduced host defense. Int J Gen Med. 2012;5:105-15. PubMed PMID: 22319248. PMCID: PMC3273373. Epub 20120131.

7. Shao L, Luo Y, Zhou D. Hematopoietic stem cell injury induced by ionizing radiation. Antioxid Redox Signal. 2014 Mar 20;20(9):1447-62. PubMed PMID: 24124731. PMCID: PMC3936513. Epub 20140210.

8. MacVittie TJ, Farese AM, Parker GA, Jackson W, 3rd, Booth C, Tudor GL, Hankey KG, Potten CS. The Gastrointestinal Subsyndrome of the Acute Radiation Syndrome in Rhesus Macaques: A Systematic Review of the Lethal Dose-response Relationship With and Without Medical Management. Health Phys. 2019 Mar;116(3):305-38. PubMed PMID: 30624353. PMCID: PMC9446380.

9. Augustine AD, Gondré-Lewis T, McBride W, Miller L, Pellmar TC, Rockwell S. Animal Models for Radiation Injury, Protection and Therapy. Radiation Research. 2005;164(1):100-9, 10.

10. Winters TA, Marzella L, Molinar-Inglis O, Price PW, Han NC, Cohen JE, Wang SJ, Fotenos AF, Sullivan JM, Esker JI, Lapinskas PJ, DiCarlo AL. Gastrointestinal

Acute Radiation Syndrome: Mechanisms, Models, Markers, and Medical Countermeasures. Radiat Res. 2024 Jun 1;201(6):628-46. PubMed PMID: 38616048. PMCID: PMC11658916.

11. Lopez M, Martin M. Medical management of the acute radiation syndrome. Rep Pract Oncol Radiother. 2011 Jul 13;16(4):138-46. PubMed PMID: 24376971. PMCID: PMC3863169. Epub 20110713.

12. Singh VK, Newman VL, Romaine PL, Wise SY, Seed TM. Radiation countermeasure agents: an update (2011-2014). Expert Opin Ther Pat. 2014 Nov;24(11):1229-55. PubMed PMID: 25315070. PMCID: PMC4438421. Epub 20141014.

13. Singh VK, Seed TM. An update on sargramostim for treatment of acute radiation syndrome. Drugs Today (Barc). 2018 Nov;54(11):679-93. PubMed PMID: 30539167.

14. Chia LA, Kuo CJ. The intestinal stem cell. Prog Mol Biol Transl Sci. 2010;96:157-73. PubMed PMID: 21075344. PMCID: PMC4165858.

15. Shaker A, Rubin DC. Intestinal stem cells and epithelial-mesenchymal interactions in the crypt and stem cell niche. Transl Res. 2010 Sep;156(3):180-7. PubMed PMID: 20801415. PMCID: PMC3019104. Epub 20100703.

16. Barker N, van Es JH, Kuipers J, Kujala P, van den Born M, Cozijnsen M, Haegebarth A, Korving J, Begthel H, Peters PJ, Clevers H. Identification of stem cells in small intestine and colon by marker gene Lgr5. Nature. 2007 Oct 25;449(7165):1003-7. PubMed PMID: 17934449. Epub 20071014.

17. Potten CS, Loeffler M. A comprehensive model of the crypts of the small intestine of the mouse provides insight into the mechanisms of cell migration and the proliferation hierarchy. J Theor Biol. 1987 Aug 21;127(4):381-91. PubMed PMID: 3328018.

18. Serrano Martinez P, Giuranno L, Vooijs M, Coppes RP. The Radiation-Induced Regenerative Response of Adult Tissue-Specific Stem Cells: Models and Signaling Pathways. Cancers (Basel). 2021 Feb 18;13(4). PubMed PMID: 33670536. PMCID: PMC7921940. Epub 20210218.

19. Goyal S, Guo CX, Singh O, Ranger A, Harrigan CF, Meade J, Luchak A, Tsang DK, Gaisano HY, Gao N, Yuzwa SA, Wrana JL, Philpott DJ, Gray-Owen SD, Girardin SE. Bacterial ADP-heptose triggers stem cell regeneration in the intestinal epithelium

following injury. Cell Stem Cell. 2025 Jul 4. PubMed PMID: 40651470. Epub 20250704.

20. Shukla PK, Gangwar R, Manda B, Meena AS, Yadav N, Szabo E, Balogh A, Lee SC, Tigyi G, Rao R. Rapid disruption of intestinal epithelial tight junction and barrier dysfunction by ionizing radiation in mouse colon in vivo: protection by N-acetyl-l-cysteine. Am J Physiol Gastrointest Liver Physiol. 2016 May 1;310(9):G705-15. PubMed PMID: 26822914. PMCID: PMC4867328. Epub 20160128.

21. Paris F, Fuks Z, Kang A, Capodieci P, Juan G, Ehleiter D, Haimovitz-Friedman A, Cordon-Cardo C, Kolesnick R. Endothelial apoptosis as the primary lesion initiating intestinal radiation damage in mice. Science. 2001 Jul 13;293(5528):293-7. PubMed PMID: 11452123.

22. Kim CK, Yang VW, Bialkowska AB. The Role of Intestinal Stem Cells in Epithelial Regeneration Following Radiation-Induced Gut Injury. Curr Stem Cell Rep. 2017;3(4):320-32. PubMed PMID: 29497599. PMCID: PMC5818549. Epub 20171005.

23. Lund PK. Fixing the breaks in intestinal stem cells after radiation: a matter of DNA damage and death or DNA repair and regeneration. Gastroenterology. 2012 Nov;143(5):1144-7. PubMed PMID: 23000480. Epub 20120919.

24. Yan KS, Chia LA, Li X, Ootani A, Su J, Lee JY, Su N, Luo Y, Heilshorn SC, Amieva MR, Sangiorgi E, Capecchi MR, Kuo CJ. The intestinal stem cell markers Bmi1 and Lgr5 identify two functionally distinct populations. Proc Natl Acad Sci U S A. 2012 Jan 10;109(2):466-71. PubMed PMID: 22190486. PMCID: PMC3258636. Epub 20111221.

25. Tian H, Biehs B, Warming S, Leong KG, Rangell L, Klein OD, de Sauvage FJ. A reserve stem cell population in small intestine renders Lgr5-positive cells dispensable. Nature. 2011 Sep 18;478(7368):255-9. PubMed PMID: 21927002. PMCID: PMC4251967. Epub 20110918.

26. Ayyaz A, Kumar S, Sangiorgi B, Ghoshal B, Gosio J, Ouladan S, Fink M, Barutcu S, Trcka D, Shen J, Chan K, Wrana JL, Gregorieff A. Single-cell transcriptomes of the regenerating intestine reveal a revival stem cell. Nature. 2019 May;569(7754):121-5. PubMed PMID: 31019301. Epub 20190424.

27. Morral C, Ayyaz A, Kuo HC, Fink M, Verginadis, II, Daniel AR, Burner DN, Driver LM, Satow S, Hasapis S, Ghinnagow R, Luo L, Ma Y, Attardi LD, Koumenis C,

Minn AJ, Wrana JL, Lee CL, Kirsch DG. p53 promotes revival stem cells in the regenerating intestine after severe radiation injury. Nat Commun. 2024 Apr 8;15(1):3018. PubMed PMID: 38589357. PMCID: PMC11001929. Epub 20240408.

28. Mauch P, Constine L, Greenberger J, Knospe W, Sullivan J, Liesveld JL, Deeg HJ. Hematopoietic stem cell compartment: acute and late effects of radiation therapy and chemotherapy. Int J Radiat Oncol Biol Phys. 1995 Mar 30;31(5):1319-39. PubMed PMID: 7713791.

29. Wu T, Pelus LM, Plett PA, Sampson CH, Chua HL, Fisher A, Feng H, Liu L, Li H, Ortiz M, Chittajallu S, Luo Q, Bhatwadekar AD, Meyer TB, Zhang X, Zhou D, Fischer KD, McKinzie DL, Miller SJ, Orschell CM. Further Characterization of Multi-Organ DEARE and Protection by 16,16 Dimethyl Prostaglandin E2 in a Mouse Model of the Hematopoietic Acute Radiation Syndrome. Radiat Res. 2023 May 1;199(5):468-89. PubMed PMID: 37014943. PMCID: PMC10278147.

30. Shao L, Li H, Pazhanisamy SK, Meng A, Wang Y, Zhou D. Reactive oxygen species and hematopoietic stem cell senescence. Int J Hematol. 2011 Jul;94(1):24-32. PubMed PMID: 21567162. PMCID: PMC3390185. Epub 20110513.

31. Singh VK, Seed TM. Repurposing Pharmaceuticals Previously Approved by Regulatory Agencies to Medically Counter Injuries Arising Either Early or Late Following Radiation Exposure. Front Pharmacol. 2021;12:624844. PubMed PMID: 34040517. PMCID: PMC8141805. Epub 20210510.

32. Dent P, Yacoub A, Fisher PB, Hagan MP, Grant S. MAPK pathways in radiation responses. Oncogene. 2003 Sep 1;22(37):5885-96. PubMed PMID: 12947395.

33. McCubrey JA, Steelman LS, Chappell WH, Abrams SL, Wong EW, Chang F, Lehmann B, Terrian DM, Milella M, Tafuri A, Stivala F, Libra M, Basecke J, Evangelisti C, Martelli AM, Franklin RA. Roles of the Raf/MEK/ERK pathway in cell growth, malignant transformation and drug resistance. Biochim Biophys Acta. 2007 Aug;1773(8):1263-84. PubMed PMID: 17126425. PMCID: PMC2696318. Epub 20061007.

34. Johnson GL, Lapadat R. Mitogen-activated protein kinase pathways mediated by ERK, JNK, and p38 protein kinases. Science. 2002 Dec 6;298(5600):1911-2. PubMed PMID: 12471242.

35. Datta SR, Dudek H, Tao X, Masters S, Fu H, Gotoh Y, Greenberg ME. Akt phosphorylation of BAD couples survival signals to the cell-intrinsic death machinery. Cell. 1997 Oct 17;91(2):231-41. PubMed PMID: 9346240.

36. Balogh A, Shimizu Y, Lee SC, Norman DD, Gangwar R, Bavaria M, Moon C, Shukla P, Rao R, Ray R, Naren AP, Banerjee S, Miller DD, Balazs L, Pelus L, Tigyi G. The autotaxin-LPA2 GPCR axis is modulated by gamma-irradiation and facilitates DNA damage repair. Cell Signal. 2015 Sep;27(9):1751-62. PubMed PMID: 26027517. PMCID: PMC4514920. Epub 20150528.

37. Wu MX, Ustyugova IV, Han L, Akilov OE. Immediate early response gene X-1, a potential prognostic biomarker in cancers. Expert Opin Ther Targets. 2013 May;17(5):593-606. PubMed PMID: 23379921. PMCID: PMC4381960. Epub 20130204.

38. Letourneux C, Rocher G, Porteu F. B56-containing PP2A dephosphorylate ERK and their activity is controlled by the early gene IEX-1 and ERK. EMBO J. 2006 Feb 22;25(4):727-38. PubMed PMID: 16456541. PMCID: PMC1383561. Epub 20060202.

39. Rocher G, Letourneux C, Lenormand P, Porteu F. Inhibition of B56-containing protein phosphatase 2As by the early response gene IEX-1 leads to control of Akt activity. J Biol Chem. 2007 Feb 23;282(8):5468-77. PubMed PMID: 17200115. Epub 20070102.

40. Brunet A, Bonni A, Zigmond MJ, Lin MZ, Juo P, Hu LS, Anderson MJ, Arden KC, Blenis J, Greenberg ME. Akt promotes cell survival by phosphorylating and inhibiting a Forkhead transcription factor. Cell. 1999 Mar 19;96(6):857-68. PubMed PMID: 10102273.

41. de Laval B, Pawlikowska P, Barbieri D, Besnard-Guerin C, Cico A, Kumar R, Gaudry M, Baud V, Porteu F. Thrombopoietin promotes NHEJ DNA repair in hematopoietic stem cells through specific activation of Erk and NF-kappaB pathways and their target, IEX-1. Blood. 2014 Jan 23;123(4):509-19. PubMed PMID: 24184684. PMCID: PMC4467873. Epub 20131101.

42. Ouellette MM, Zhou S, Yan Y. Cell Signaling Pathways That Promote Radioresistance of Cancer Cells. Diagnostics (Basel). 2022 Mar 8;12(3). PubMed PMID: 35328212. PMCID: PMC8947583. Epub 20220308.

43. Deng W, Wang DA, Gosmanova E, Johnson LR, Tigyi G. LPA protects intestinal epithelial cells from apoptosis by inhibiting the mitochondrial pathway. Am J Physiol Gastrointest Liver Physiol. 2003 May;284(5):G821-9. PubMed PMID: 12684213.

44. Shen L, Zhi L, Hu W, Wu MX. IEX-1 targets mitochondrial F1Fo-ATPase inhibitor for degradation. Cell Death Differ. 2009 Apr;16(4):603-12. PubMed PMID: 19096392. PMCID: PMC2696391. Epub 20081219.

45. Ye X, Ishii I, Kingsbury MA, Chun J. Lysophosphatidic acid as a novel cell survival/apoptotic factor. Biochim Biophys Acta. 2002 Dec 30;1585(2-3):108-13. PubMed PMID: 12531543.

46. E S, Lai YJ, Tsukahara R, Chen CS, Fujiwara Y, Yue J, Yu JH, Guo H, Kihara A, Tigyi G, Lin FT. Lysophosphatidic acid 2 receptor-mediated supramolecular complex formation regulates its antiapoptotic effect. J Biol Chem. 2009 May 22;284(21):14558-71. PubMed PMID: 19293149. PMCID: PMC2682904. Epub 20090317.

47. Oh YS, Jo NW, Choi JW, Kim HS, Seo SW, Kang KO, Hwang JI, Heo K, Kim SH, Kim YH, Kim IH, Kim JH, Banno Y, Ryu SH, Suh PG. NHERF2 specifically interacts with LPA2 receptor and defines the specificity and efficiency of receptor-mediated phospholipase C-beta3 activation. Mol Cell Biol. 2004 Jun;24(11):5069-79. PubMed PMID: 15143197. PMCID: PMC416407.

48. Lukas J, Lukas C, Bartek J. More than just a focus: The chromatin response to DNA damage and its role in genome integrity maintenance. Nat Cell Biol. 2011 Oct 3;13(10):1161-9. PubMed PMID: 21968989. Epub 20111003.

49. Deng W, Kimura Y, Gududuru V, Wu W, Balogh A, Szabo E, Thompson KE, Yates CR, Balazs L, Johnson LR, Miller DD, Strobos J, McCool WS, Tigyi GJ. Mitigation of the hematopoietic and gastrointestinal acute radiation syndrome by octadecenyl thiophosphate, a small molecule mimic of lysophosphatidic acid. Radiat Res. 2015 Apr;183(4):465-75. PubMed PMID: 25807318. PMCID: PMC4428663. Epub 20150325.

50. Deng W, Shuyu E, Tsukahara R, Valentine WJ, Durgam G, Gududuru V, Balazs L, Manickam V, Arsura M, VanMiddlesworth L, Johnson LR, Parrill AL, Miller DD, Tigyi G. The lysophosphatidic acid type 2 receptor is required for protection against radiation-induced intestinal injury. Gastroenterology. 2007 May;132(5):1834-51. PubMed PMID: 17484878. PMCID: PMC3446791. Epub 20070324.

51. Lin FT, Lai YJ, Makarova N, Tigyi G, Lin WC. The lysophosphatidic acid 2 receptor mediates down-regulation of Siva-1 to promote cell survival. J Biol Chem. 2007 Dec 28;282(52):37759-69. PubMed PMID: 17965021. PMCID: PMC3496872. Epub 20071026.

52. Patil R, Szabo E, Fells JI, Balogh A, Lim KG, Fujiwara Y, Norman DD, Lee SC, Balazs L, Thomas F, Patil S, Emmons-Thompson K, Boler A, Strobos J, McCool SW, Yates CR, Stabenow J, Byrne GI, Miller DD, Tigyi GJ. Combined mitigation of the gastrointestinal and hematopoietic acute radiation syndromes by an LPA2 receptor-specific nonlipid agonist. Chem Biol. 2015 Feb 19;22(2):206-16. PubMed PMID: 25619933. PMCID: PMC4336611. Epub 20150122.

53. Shukla PK, Meena AS, Gangwar R, Szabo E, Balogh A, Chin Lee S, Vandewalle A, Tigyi G, Rao R. LPAR2 receptor activation attenuates radiation-induced disruption of apical junctional complexes and mucosal barrier dysfunction in mouse colon. FASEB J. 2020 Sep;34(9):11641-57. PubMed PMID: 32654268. PMCID: PMC7725959. Epub 20200712.

54. Liu W, Hopkins AM, Hou J. The development of modulators for lysophosphatidic acid receptors: A comprehensive review. Bioorg Chem. 2021 Dec;117:105386. PubMed PMID: 34695732. Epub 20211004.

55. Patil R, Fells JI, Szabo E, Lim KG, Norman DD, Balogh A, Patil S, Strobos J, Miller DD, Tigyi GJ. Design and synthesis of sulfamoyl benzoic acid analogues with subnanomolar agonist activity specific to the LPA2 receptor. J Med Chem. 2014 Aug 28;57(16):7136-40. PubMed PMID: 25100502. PMCID: PMC4148159. Epub 20140812.

56. Kuo B, Szabo E, Lee SC, Balogh A, Norman D, Inoue A, Ono Y, Aoki J, Tigyi G. The LPA(2) receptor agonist Radioprotectin-1 spares Lgr5-positive intestinal stem cells from radiation injury in murine enteroids. Cell Signal. 2018 Nov;51:23-33. PubMed PMID: 30063964. PMCID: PMC6163127. Epub 20180729.

57. Norman DD, Lee SC, Shin Y, Ibrahim MM, Jablonski MM, Wang Y, Balazs L, Davies EW, Benyo Z, Tigyi GJ. Development of an Extended-release Formulation of Radioprotectin-1 for Mitigation of Gastrointestinal Acute Radiation Syndrome. Radiat Res. 2026 Jan 27. PubMed PMID: 41592715. Epub 20260127.

58. Citrin D, Cotrim AP, Hyodo F, Baum BJ, Krishna MC, Mitchell JB. Radioprotectors and mitigators of radiation-induced normal tissue injury. Oncologist. 2010;15(4):360-71. PubMed PMID: 20413641. PMCID: PMC3076305.

59. Ibrahim MM, Maria DN, Mishra SR, Guragain D, Wang X, Jablonski MM. Once Daily Pregabalin Eye Drops for Management of Glaucoma. ACS Nano. 2019 Dec 24;13(12):13728-44. PubMed PMID: 31714057. PMCID: PMC7785203. Epub 20191118.

60. Ibrahim MM, Maria DN, Wang X, Simpson RN, Hollingsworth TJ, Jablonski MM. Enhanced Corneal Penetration of a Poorly Permeable Drug Using Bioadhesive Multiple Microemulsion Technology. Pharmaceutics. 2020 Jul 26;12(8). PubMed PMID: 32722550. PMCID: PMC7463957. Epub 20200726.

61. Maria DN, Ibrahim MM, Kim MJ, Maria SN, White WA, Wang X, Hollingsworth TJ, Jablonski MM. Evaluation of Pregabalin bioadhesive multilayered microemulsion IOP-lowering eye drops. J Control Release. 2024 Sep;373:667-87. PubMed PMID: 39079659. PMCID: PMC11384292. Epub 20240801.

62. Lawrence MJ, Rees GD. Microemulsion-based media as novel drug delivery systems. Adv Drug Deliv Rev. 2000 Dec 6;45(1):89-121. PubMed PMID: 11104900.

63. Constantinides PP. Lipid microemulsions for improving drug dissolution and oral absorption: physical and biopharmaceutical aspects. Pharm Res. 1995 Nov;12(11):1561-72. PubMed PMID: 8592652.

64. Kondratyev AD, Chung KN, Jung MO. Identification and characterization of a radiation-inducible glycosylated human early-response gene. Cancer Res. 1996 Apr 1;56(7):1498-502. PubMed PMID: 8603392.

65. Arlt A, Schafer H. Role of the immediate early response 3 (IER3) gene in cellular stress response, inflammation and tumorigenesis. Eur J Cell Biol. 2011 Jun-Jul;90(6-7):545-52. PubMed PMID: 21112119. Epub 20101126.

66. Garcia J, Ye Y, Arranz V, Letourneux C, Pezeron G, Porteu F. IEX-1: a new ERK substrate involved in both ERK survival activity and ERK activation. EMBO J. 2002 Oct 1;21(19):5151-63. PubMed PMID: 12356731. PMCID: PMC129026.

67. Kumar R, Lutz W, Frank E, Im HJ. Immediate early gene X-1 interacts with proteins that modulate apoptosis. Biochem Biophys Res Commun. 2004 Oct 29;323(4):1293-8. PubMed PMID: 15451437. PMCID: PMC2895269.

68. Arlt A, Rosenstiel P, Kruse ML, Grohmann F, Minkenberg J, Perkins ND, Folsch UR, Schreiber S, Schafer H. IEX-1 directly interferes with RelA/p65 dependent transactivation and regulation of apoptosis. Biochim Biophys Acta. 2008 May;1783(5):941-52. PubMed PMID: 18191642. Epub 20071223.

69. Deng W, Balazs L, Wang DA, Van Middlesworth L, Tigyi G, Johnson LR. Lysophosphatidic acid protects and rescues intestinal epithelial cells from radiation- and chemotherapy-induced apoptosis. Gastroenterology. 2002 Jul;123(1):206-16. PubMed PMID: 12105849.

70. Sommer SL, Berndt TJ, Frank E, Patel JB, Redfield MM, Dong X, Griffin MD, Grande JP, van Deursen JM, Sieck GC, Romero JC, Kumar R. Elevated blood pressure and cardiac hypertrophy after ablation of the gly96/IEX-1 gene. J Appl Physiol (1985). 2006 Feb;100(2):707-16. PubMed PMID: 16166241. Epub 20050915.

71. Ghaleb AM, McConnell BB, Kaestner KH, Yang VW. Altered intestinal epithelial homeostasis in mice with intestine-specific deletion of the Kruppel-like factor 4 gene. Dev Biol. 2011 Jan 15;349(2):310-20. PubMed PMID: 21070761. PMCID: PMC3022386. Epub 20101109.

72. Gong W, Guo M, Han Z, Wang Y, Yang P, Xu C, Wang Q, Du L, Li Q, Zhao H, Fan F, Liu Q. Mesenchymal stem cells stimulate intestinal stem cells to repair radiation-induced intestinal injury. Cell Death Dis. 2016 Sep 29;7(9):e2387. PubMed PMID: 27685631. PMCID: PMC5059875. Epub 20160929.

73. Mahe MM, Aihara E, Schumacher MA, Zavros Y, Montrose MH, Helmrath MA, Sato T, Shroyer NF. Establishment of Gastrointestinal Epithelial Organoids. Curr Protoc Mouse Biol. 2013 Dec 19;3(4):217-40. PubMed PMID: 25105065. PMCID: PMC4120977. Epub 20131219.

74. Versteeg HH, Nijhuis E, van den Brink GR, Evertzen M, Pynaert GN, van Deventer SJ, Coffer PJ, Peppelenbosch MP. A new phosphospecific cell-based ELISA for p42/p44 mitogen-activated protein kinase (MAPK), p38 MAPK, protein kinase B and cAMP-response-element-binding protein. Biochem J. 2000 Sep 15;350 Pt 3(Pt 3):717-22. PubMed PMID: 10970784. PMCID: PMC1221302.

75. Kramer C, Nahmias Z, Norman DD, Mulvihill TA, Coons LB, Cole JA. Dermacentor variabilis: regulation of fibroblast migration by tick salivary gland extract

and saliva. Exp Parasitol. 2008 Jul;119(3):391-7. PubMed PMID: 18492598. Epub 20080414.

76. Oami T, Abtahi S, Shimazui T, Chen CW, Sweat YY, Liang Z, Burd EM, Farris AB, Roland JT, Tsukita S, Ford ML, Turner JR, Coopersmith CM. Claudin-2 upregulation enhances intestinal permeability, immune activation, dysbiosis, and mortality in sepsis. Proc Natl Acad Sci U S A. 2024 Mar 5;121(10):e2217877121. PubMed PMID: 38412124. PMCID: PMC10927519. Epub 20240227.

77. Kirsch DG, Santiago PM, di Tomaso E, Sullivan JM, Hou WS, Dayton T, Jeffords LB, Sodha P, Mercer KL, Cohen R, Takeuchi O, Korsmeyer SJ, Bronson RT, Kim CF, Haigis KM, Jain RK, Jacks T. p53 controls radiation-induced gastrointestinal syndrome in mice independent of apoptosis. Science. 2010 Jan 29;327(5965):593-6. PubMed PMID: 20019247. PMCID: PMC2897160. Epub 20091217.

78. Arlt A, Grobe O, Sieke A, Kruse ML, Folsch UR, Schmidt WE, Schafer H. Expression of the NF-kappa B target gene IEX-1 (p22/PRG1) does not prevent cell death but instead triggers apoptosis in Hela cells. Oncogene. 2001 Jan 4;20(1):69-76. PubMed PMID: 11244505.

79. Zhang Y, Chen X, Wang X, Chen J, Du C, Wang J, Liao W. Insights into ionizing radiation-induced bone marrow hematopoietic stem cell injury. Stem Cell Res Ther. 2024 Jul 23;15(1):222. PubMed PMID: 39039566. PMCID: PMC11265359. Epub 20240723.

80. Azzam EI, Jay-Gerin JP, Pain D. Ionizing radiation-induced metabolic oxidative stress and prolonged cell injury. Cancer Lett. 2012 Dec 31;327(1-2):48-60. PubMed PMID: 22182453. PMCID: PMC3980444. Epub 20111217.

81. Singh VK, Romaine PL, Seed TM. Medical Countermeasures for Radiation Exposure and Related Injuries: Characterization of Medicines, FDA-Approval Status and Inclusion into the Strategic National Stockpile. Health Phys. 2015 Jun;108(6):607-30. PubMed PMID: 25905522. PMCID: PMC4418776.

9. Bibliography of the Candidate's Publications

Cumulative impact factor of journals listed: 187.86

Related to the thesis (**Total IF: 6.088**):

1. **Norman DD**, Shin Y, Balázs L, Benyo Z, Lee SC, Tigyi GJ. Loss of the lysophosphatidic acid-induced immediate early gene IEX-1 exacerbates acute radiation syndrome. Radiat Res. 2026. Submitted under review. (**IF: 2.7**)
2. **Norman DD**, Lee SC, Shin Y, Ibrahim MM, Jablonski MM, Wang Y, Balázs L, Davies EW, Benyo Z, Tigyi GJ. Development of an Extended-release Formulation of Radioprotectin-1 for Mitigation of Gastrointestinal Acute Radiation Syndrome. Radiat Res. 2026. (**IF: 2.7**)
3. Kuo B, Szabo E, Lee SC, Balogh A, **Norman D**, Inoue A, Ono Y, Aoki J, Tigyi G. The LPA(2) receptor agonist Radioprotectin-1 spares Lgr5-positive intestinal stem cells from radiation injury in murine enteroids. Cell Signal. 2018;51:23-33. (**IF: 3.388**)

Not related to the thesis (**Total IF: 181.772**):

1. Rai P, Clark CJ, Kardam V, Womack CB, Thammathong J, **Norman DD**, Tigyi GJ, Bicker K, Weissmiller AM, Dubey KD, Banerjee S. Structure-Based Discovery of MolPort-137: A Novel Autotaxin Inhibitor That Improves Paclitaxel Efficacy. Int J Mol Sci. 2025;26(2). (**IF: 4.9**)
2. Dacheux MA, **Norman DD**, Shin Y, Tigyi GJ, Lee SC. Deleting autotaxin in LysM+ myeloid cells impairs innate tumor immunity in models of metastatic melanoma. iScience. 2024;27(10):110971. (**IF: 4.1**)
3. Hutka B, Varallyay A, Laszlo SB, Toth AS, Scheich B, Paku S, Voros I, Pos Z, Varga ZV, **Norman DD**, Balogh A, Benyo Z, Tigyi G, Gyires K, Zadori ZS. A dual role of lysophosphatidic acid type 2 receptor (LPAR2) in nonsteroidal anti-inflammatory drug-induced mouse enteropathy. Acta Pharmacol Sin. 2024;45(2):339-53. (**IF: 8.4**)
4. Kim TY, Kim A, Aryal YP, Sung S, Pokharel E, Neupane S, Choi SY, Ha JH, Jung JK, Yamamoto H, An CH, Suh JY, Sohn WJ, Lee Y, Jang IH, **Norman DD**, Tigyi GJ, An SY, Kim JY. Functional modulation of lysophosphatidic acid type 2 G-

protein coupled receptor facilitates alveolar bone formation. J Cell Physiol. 2024;239(1):112-23. (**IF: 4.0**)

5. Rai P, Clark CJ, Womack CB, Dearing C, Thammathong J, **Norman DD**, Tigyi GJ, Sen S, Bicker K, Weissmiller AM, Banerjee S. Novel Autotaxin Inhibitor ATX-1d Significantly Enhances Potency of Paclitaxel-An In Silico and In Vitro Study. Molecules. 2024;29(18). (**IF: 4.6**)
6. Dacheux MA, **Norman DD**, Tigyi GJ, Lee SC. Emerging roles of lysophosphatidic acid receptor subtype 5 (LPAR5) in inflammatory diseases and cancer. Pharmacol Ther. 2023;245:108414. (**IF: 12.0**)
7. Heo SC, Keum BR, Seo EJ, Yoon J, Jeong S, Tigyi GJ, **Norman D**, Jang IH, Kim HJ. Lysophosphatidic acid induces proliferation and osteogenic differentiation of human dental pulp stem cell through lysophosphatidic acid receptor 3/extracellular signal-regulated kinase signaling axis. J Dent Sci. 2023;18(3):1219-26. (**IF: 3.4**)
8. Lin KH, Lee SC, Dacheux MA, **Norman DD**, Balogh A, Bavaria M, Lee H, Tigyi G. E2F7 drives autotaxin/Enpp2 transcription via chromosome looping: Repression by p53 in murine but not in human carcinomas. FASEB J. 2023;37(7):e23058. (**IF: 4.4**)
9. Banerjee S, Lee S, **Norman DD**, Tigyi GJ. Designing Dual Inhibitors of Autotaxin-LPAR GPCR Axis. Molecules. 2022;27(17). (**IF: 4.6**)
10. Dacheux MA, Lee SC, Shin Y, **Norman DD**, Lin KH, E S, Yue J, Benyo Z, Tigyi GJ. Prometastatic Effect of ATX Derived from Alveolar Type II Pneumocytes and B16-F10 Melanoma Cells. Cancers (Basel). 2022;14(6). (**IF: 5.2**)
11. Lee SC, Lin KH, Balogh A, **Norman DD**, Bavaria M, Kuo B, Yue J, Balazs L, Benyo Z, Tigyi G. Dysregulation of lysophospholipid signaling by p53 in malignant cells and the tumor microenvironment. Cell Signal. 2021;78:109850. (**IF: 4.85**)
12. Tigyi G, Dacheux MA, Lin KH, Yue J, **Norman D**, Benyo Z, Lee SC. Anti-cancer strategies targeting the autotaxin-lysophosphatidic acid receptor axis: is there a path forward? Cancer Metastasis Rev. 2021;40(1):3-5.
13. Banerjee S, **Norman DD**, Deng S, Fakayode SO, Lee SC, Parrill AL, Li W, Miller DD, Tigyi GJ. Molecular modelling guided design, synthesis and QSAR analysis of new small molecule non-lipid autotaxin inhibitors. Bioorg Chem. 2020;103:104188. (**IF: 5.275**)

14. Lee SC, Dacheux MA, **Norman DD**, Balazs L, Torres RM, Augelli-Szafran CE, Tigyi GJ. Regulation of Tumor Immunity by Lysophosphatidic Acid. Cancers (Basel). 2020;12(5). (**IF: 6.639**)
15. Morstein J, Dacheux MA, **Norman DD**, Shemet A, Donthamsetti PC, Citir M, Frank JA, Schultz C, Isacoff EY, Parrill AL, Tigyi GJ, Trauner D. Optical Control of Lysophosphatidic Acid Signaling. J Am Chem Soc. 2020;142(24):10612-6. (**IF: 15.419**)
16. Flammier S, Peyruchaud O, Bourguillault F, Duboeuf F, Davignon JL, **Norman DD**, Isaac S, Marotte H, Tigyi G, Machuca-Gayet I, Coury F. Osteoclast-Derived Autotaxin, a Distinguishing Factor for Inflammatory Bone Loss. Arthritis Rheumatol. 2019;71(11):1801-11. (**IF: 9.586**)
17. Morstein J, Hill RZ, Novak AJE, Feng S, **Norman DD**, Donthamsetti PC, Frank JA, Harayama T, Williams BM, Parrill AL, Tigyi GJ, Riezman H, Isacoff EY, Bautista DM, Trauner D. Optical control of sphingosine-1-phosphate formation and function. Nat Chem Biol. 2019;15(6):623-31. (**IF: 12.587**)
18. Tigyi GJ, Yue J, **Norman DD**, Szabo E, Balogh A, Balazs L, Zhao G, Lee SC. Regulation of tumor cell - Microenvironment interaction by the autotaxin-lysophosphatidic acid receptor axis. Adv Biol Regul. 2019;71:183-93.
19. Tigyi GJ, Johnson LR, Lee SC, **Norman DD**, Szabo E, Balogh A, Thompson K, Boler A, McCool WS. Lysophosphatidic acid type 2 receptor agonists in targeted drug development offer broad therapeutic potential. J Lipid Res. 2019;60(3):464-74. (**IF: 4.483)**
20. Banerjee S, **Norman DD**, Lee SC, Parrill AL, Pham TC, Baker DL, Tigyi GJ, Miller DD. Highly Potent Non-Carboxylic Acid Autotaxin Inhibitors Reduce Melanoma Metastasis and Chemotherapeutic Resistance of Breast Cancer Stem Cells. J Med Chem. 2017;60(4):1309-24. (**IF: 6.253**)
21. Ragle LE, Palanisamy DJ, Joe MJ, Stein RS, **Norman DD**, Tigyi G, Baker DL, Parrill AL. Discovery and synthetic optimization of a novel scaffold for hydrophobic tunnel-targeted autotaxin inhibition. Bioorg Med Chem. 2016;24(19):4660-74. (**IF: 2.930**)
22. Balogh A, Shimizu Y, Lee SC, **Norman DD**, Gangwar R, Bavaria M, Moon C, Shukla P, Rao R, Ray R, Naren AP, Banerjee S, Miller DD, Balazs L, Pelus L, Tigyi

G. The autotaxin-LPA2 GPCR axis is modulated by gamma-irradiation and facilitates DNA damage repair. Cell Signal. 2015;27(9):1751-62. (**IF: 4.191**)

23. Lee SC, Fujiwara Y, Liu J, Yue J, Shimizu Y, **Norman DD**, Wang Y, Tsukahara R, Szabo E, Patil R, Banerjee S, Miller DD, Balazs L, Ghosh MC, Waters CM, Oravecz T, Tigyi GJ. Autotaxin and LPA1 and LPA5 receptors exert disparate functions in tumor cells versus the host tissue microenvironment in melanoma invasion and metastasis. Mol Cancer Res. 2015;13(1):174-85. (**IF: 4.510**)
24. Patil R, Szabo E, Fells JI, Balogh A, Lim KG, Fujiwara Y, **Norman DD**, Lee SC, Balazs L, Thomas F, Patil S, Emmons-Thompson K, Boler A, Strobos J, McCool SW, Yates CR, Stabenow J, Byrne GI, Miller DD, Tigyi GJ. Combined mitigation of the gastrointestinal and hematopoietic acute radiation syndromes by an LPA2 receptor-specific nonlipid agonist. Chem Biol. 2015;22(2):206-16. (**IF: 5.774**)
25. Fells JI, Lee SC, **Norman DD**, Tsukahara R, Kirby JR, Nelson S, Seibel W, Papoian R, Patil R, Miller DD, Parrill AL, Pham TC, Baker DL, Bittman R, Tigyi G. Targeting the hydrophobic pocket of autotaxin with virtual screening of inhibitors identifies a common aromatic sulfonamide structural motif. FEBS J. 2014;281(4):1017-28. (**IF: 4.001**)
26. Leblanc R, Lee SC, David M, Bordet JC, **Norman DD**, Patil R, Miller D, Sahay D, Ribeiro J, Clezardin P, Tigyi GJ, Peyruchaud O. Interaction of platelet-derived autotaxin with tumor integrin alphaVbeta3 controls metastasis of breast cancer cells to bone. Blood. 2014;124(20):3141-50. (**IF: 10.452**)
27. Morales-Lazaro SL, Serrano-Flores B, Llorente I, Hernandez-Garcia E, Gonzalez-Ramirez R, Banerjee S, Miller D, Gududuru V, Fells J, **Norman D**, Tigyi G, Escalante-Alcalde D, Rosenbaum T. Structural determinants of the transient receptor potential 1 (TRPV1) channel activation by phospholipid analogs. J Biol Chem. 2014;289(35):24079-90. (**IF: 4.573**)
28. Patil R, Fells JI, Szabo E, Lim KG, **Norman DD**, Balogh A, Patil S, Strobos J, Miller DD, Tigyi GJ. Design and synthesis of sulfamoyl benzoic acid analogues with subnanomolar agonist activity specific to the LPA2 receptor. J Med Chem. 2014;57(16):7136-40. (**IF: 5.447**)
29. Fells JI, Lee SC, Fujiwara Y, **Norman DD**, Lim KG, Tsukahara R, Liu J, Patil R, Miller DD, Kirby RJ, Nelson S, Seibel W, Papoian R, Parrill AL, Baker DL, Bittman

R, Tigyi G. Hits of a high-throughput screen identify the hydrophobic pocket of autotaxin/lysophospholipase D as an inhibitory surface. Mol Pharmacol. 2013;84(3):415-24. (**IF: 4.120**)

30. **Norman DD**, Ibezim A, Scott WE, White S, Parrill AL, Baker DL. Autotaxin inhibition: development and application of computational tools to identify site-selective lead compounds. Bioorg Med Chem. 2013;21(17):5548-60. (**IF: 2.951**)
31. Ren F, Bhana S, **Norman DD**, Johnson J, Xu L, Baker DL, Parrill AL, Huang X. Gold nanorods carrying paclitaxel for photothermal-chemotherapy of cancer. Bioconjug Chem. 2013;24(3):376-86. (**IF: 4.821**)
32. Bolen AL, Naren AP, Yarlagadda S, Beranova-Giorgianni S, Chen L, **Norman D**, Baker DL, Rowland MM, Best MD, Sano T, Tsukahara T, Liliom K, Igarashi Y, Tigyi G. The phospholipase A1 activity of lysophospholipase A-I links platelet activation to LPA production during blood coagulation. J Lipid Res. 2011;52(5):958-70. (**IF: 5.559**)
33. Kramer C, Nahmias Z, **Norman DD**, Mulvihill TA, Coons LB, Cole JA. Dermacentor variabilis: regulation of fibroblast migration by tick salivary gland extract and saliva. Exp Parasitol. 2008;119(3):391-7. (**IF: 1.751**)

10. Acknowledgements

I would like to express my deepest gratitude to my mentor and supervisor, Professor Gábor Tigyi, for his unwavering support and guidance. I would also like to thank Professor Zoltán Benyó for his insight, guidance, and the opportunity to advance my education. I would like to express special thanks to Professor Sue Chin Lee for years of invaluable knowledge, advice, training, and camaraderie. I also deeply appreciate the efforts and dedication of my co-authors, coworkers, and collaborators, with special thanks to Yoojin Shin for her tireless efforts in facilitating this work. Finally, I would like to thank my family for their unending support and encouragement throughout my journey.